ELEC5881M Final Report

Co-simulation of Smart Grid and Communication Network

Etinosa Ekomwenrenren

Student ID: 200990550

Submitted in accordance with the requirements for the degree of
Master of Science
in Electrical Engineering and Renewable Energy Systems

Supervisor: Dr Petros Aristidou

Assessor: Dr Li X Zhang

The University of Leeds

School of Electronic and Electrical Engineering

April 2017

Declaration of Academic Integrity

The candidate confirms that the work submitted is his/her own, except where work which has formed part of jointly-authored publications has been included. The contribution of the candidate and the other authors to this work has been explicitly indicated in the report. The candidate confirms that appropriate credit has been given within the report where reference has been made to the work of others.

This copy has been supplied on the understanding that no quotation from the report may be published without proper acknowledgement. The candidate, however, confirms his/her consent to the University of Leeds copying and distributing all or part of this work in any forms and using third parties, who might be outside the University, to monitor breaches of regulations, to verify whether this work contains plagiarised material, and for quality assurance purposes.

The candidate confirms that the details of any mitigating circumstances have been submitted to the Student Support Office at the School of Electronic and Electrical Engineering, at the University of Leeds.

Etinosa Ekomwenrenren

26/04/2017

Table of Contents

Abstract

The current electrical power grid relies on non-renewable resources that damage the environment, is inefficient, and is incapable of meeting future demand growth. To solve these challenges, the grid is undergoing modernisation to become smarter and greener.

This modernisation of the grid will involve extensive use of communication and information technology. Because of this proliferation of communication networks in the power system, it has become imperative to determine whether degradations in the power system's performance arise due to these interactions.

Hence, this project aims to examine the effect of these interactions on the stability of the power grid by jointly simulating the dynamics of the power system with the underlying communication architecture. Specifically, this was done by examining the effects of communication delays on the performance of a wide area damping controller (WADC). A reduced Great Britain transmission network model was utilised as the test system.

Simulation results show that communication delays degrade the performance of the WADC and may lead to small-signal instability in some cases.

List of Abbreviations

Abbreviations	Meaning
AMI	Advanced metering infrastructure
AVR	Automatic Voltage Regulator
BAN	Building Area Network
BPSK	Binary Phase Shift Keying
CCGT	Combine Cycle Gas Turbine
CDMA	Code-Division Multiple Access
CIM	Common Information Model
DGD	Differential Group Delay
DNP3	Distributed Network Protocol
EDFA	Erbium-Doped Fibre Amplifier
EMS	Energy Management Systems
FAN	Field Area Network
GPRS	General Packet Radio Service
GVD	Group Velocity Dispersion
HAN	Home Area Network
IAN	Industrial Area Network
ICCP	Inter-Control Centre Protocol
IP	Internet Protocol
LTE	Long-Term Evolution
MPLS	Multiprotocol Label Switching
NAN	Neighbourhood Area Network
NGET	National Grid Electricity Transmission
NLSE	Nonlinear Schroedinger's Equation
PID	Proportional-Integral-Derivative
PLC	Powerline Communications
PMU	Phasor Measurement Unit
PSS	Power System Stabilizer
RGBN	Representative Great Britain Network
SCADA	Supervisory Control and Data acquisition
SONET	Synchronous Optical Networking
SVC	Static VAR Compensator
TASE	Tele-control Application Service Element
UHF	Ultra High Frequency

WAMS	Wide Area Monitoring Systems
WAN	Wide Area Network
WiMAX	Worldwide Interoperability for Microwave Access
WDM	Wavelength-Division Multiplexing

List of Figures

List of Tables

Chapter 1
Introduction

1.1 Background and project justification

The current grid is incapable of meeting the growth in energy demand without modernisation. The grid presently relies on non-renewable resources (such as fossil fuels) that are rapidly depleting and causing immense harm to the environment.

Also, the present grid lacks visibility, with the unavailability of real-time high resolution information necessary to make critical decisions hampering situational awareness and resulting in blackouts [1].

Furthermore, the current grid has inefficient power storage resulting in the real-time matching of supply with demand, leading to high strain on the infrastructure during peak demand hours.

To solve these challenges and meet future demand growth, the traditional electric power grid needs to become more intelligent and flexible. The grid of the future will be smart and green. And this will be made possible by using information and communication technology extensively [2], [3].

The pervasive use of information and communication technology will allow communication between the customer premises and the traditional transmission and distribution architecture, resulting in a grid that is capable of operating with bi-directional flow of electric energy. This will give utilities the ability to adjust customer's load demands and allow them finer control over distributed energy resources and storage. An upshot of this will be better integration of distributed energy resources that will result in increased penetration of renewable resources and reduced reliance on fossil fuels.

The communication infrastructure of the smart grid will provide better interconnection of grid components and assets dispersed across wide geographical areas [4]. This will result in improved monitoring and automatic control of the entire grid. Because of the improved situational awareness, real-time monitoring of the power system dynamic health will become a possibility, reducing the likelihood of outages and catastrophic blackouts [1], [5].

To realise these innovative features of the smart grid, communication networks will become more widespread, and the volume and instances of information flow in the grid will increase substantially.

This proliferation of communication devices is not without its downsides, however. One of the challenges of the increased role of communication is cyber security [6]. With the increased use of wide area measurements for controlling voltage, maintaining generator synchronism, and for automating generation control [7], attacks on the communication infrastructure may threaten the stable and reliable operation of the power system. For example, attacks could be made on the time delays of the communication networks used in automatic generation control (AGC) and wide area damping controls (WADC) [7], [8], or on the measurements from phasor measurement units (PMUs) used for power system state estimation functions [9].

As a result, it is vital to understand how the cyber communication systems will interact with the power system (which is in the physical domain).

Simulation offers a cost effective and safe way to study this interaction and to assess the effect on the grid operation due to the communication networks.

Consequently, this project co-simulated the communication network with the power system in order to assess changes in the operational performance of the power system owing to the effects of the communication network. In particular, we have investigated the effects the communication network has on the small-signal stability of a geographically dispersed transmission power system controlled by a wide-area damping controller.

To achieve this, we have implemented a reduced dynamic model of the Great Britain transmission network [10], [11] overlaid with the UK (BT) core fibre network [12]. `Using the communication architecture, we designed a wide area damping controller using robust H_∞ based techniques with regional pole placement. The small-signal stability of the combined system was then analysed with eigenvalue analysis for different loading and network traffic scenarios.

From the investigations, it was observed that the time delays from the communication network can make the system unstable in the small, depending on the wide area design objectives. Additionally, for all scenarios investigated, the communication time delays result in a consequential degradation in the performance of the wide area damping controller.

1.2 Aims/objectives of the project

The objectives of this project include the following:

- To implement a dynamic model of the representative Great Britain transmission network (RGBN);
- To model a communication network;

- To jointly simulate the communication network and power system in a single environment;
- To design a centralised wide area damping controller for damping the rotor oscillations of the power system;
- To investigate the effect of the communication network on the small-signal stability of the power system with the wide area damping controller in operation.

1.3 Contributions of the project

- Co-simulated the UK (BT) core fibre network and a dynamic model a representative Great Britain transmission network on MATLAB/Simulink;
- Illustrated the procedures for a systematic design of a wide area controller and shown its effectiveness for damping both intra-station and inter-area oscillations;
- Shown that H_∞ control with pole placement can be used to synthesise a wide area damping controller that is robust to changes in power system loading conditions;
- Demonstrated the effects of time delays on a power system with only wide area damping control and with both wide area damping control and local power system stabilizer using both eigenvalues analysis and nonlinear time domain simulations.

1.4 Scope

This work considers the effect of communication delays on the power system small-signal stability.

1.5 Report outline

The remainder of this report is organised as follows. Chapter two reviews the literature on power systems communication and the techniques for co-simulating the power system and communication network. Chapter three details how the power system is modelled and describes the communication topology used in this study. Simulations of the modelled systems and discussion of results obtained are presented in the fourth chapter. Chapter five concludes the work, providing a summary of the work and outlining further research directions.

Chapter 2
Literature Review

2.1 Power system communications

The operation of the electric grid increasingly depends on communication services. These services allow for the real-time automation and control of the generation, transmission, and distribution systems, with recent advances providing for customer interaction with the advent of smart metering and demand response. Protection relay communication and substation automation, inter-platform applications, distribution grid automation and customer communications, and supervisory and wide area monitoring and control systems are some of the communication functions in the traditional electric grid [13].

2.1.1 Substation automation and protection relay communication

These communication applications entail fast automated systems that provide control and protection /for power system equipment in substations, switchyards, and generating plants. Very stringent security and reliability requirements, along with low latency constraints, are imposed on the communication networks used for this application [14]. Due to these requirements, dedicated telecommunication infrastructures are usually employed. IEEE 1646 standards provide the timing requirements and the IEC 61850 standard specify the communication requirement for functions and device models [2].

Table 2.1 Standard requirements for timing of substation automation communications services [2]

Information Types	External to substation	Internal to substation
Operations and maintenance information	10 seconds	1 second
Monitoring and control information	1 second	16 milliseconds
Protection information	8-12 milliseconds	4 milliseconds
Image files	1 minute	10 seconds
Program files	10 minutes	1 minute
Processed data files	30 seconds	10 milliseconds
Text strings	10 seconds	2 seconds

2.1.2 Supervisory and wide area monitoring and control systems

Status information and measurement data from the grid are sent through this communication systems to the control centres and actionable commands are transmitted back to remedy the situation. This usually comprises the power system supervisory control and data acquisition (SCADA) and related surveillance applications, including wide area monitoring systems (WAMS) [13] [14].

A broadband private network (e.g., optical fibre) is normally used for transmission grid SCADA, while distribution network SCADA (in particular for medium voltage grids) can be implemented through wireless services such as long-term evolution (LTE) and general packet radio service (GPRS) [13].

The synchrophasor-based wide are monitoring systems, which involves sending synchronised phasor data of power system parameters to the control-centres, have different communication requirements depending on the specific wide area application being provided. Some of these communication requirements are shown in Table 2.1.

The power system SCADA uses the standardised communication protocol IEC 60870-5, other legacy and industry protocols such as Modbus and DNP3 exists [15]. The defines a profile for communicating control messages between circuit-switched systems [16]. The IEC 60870-5-104 protocol (which is an extension of IEC 60870-5-101) provides changes in layer services and uses the open TCP/IP interface [16].

The IEEE C37.118 specifies the data format and general operation of the phasor measurement unit (PMU) [13].

2.1.3 Inter-platform applications

This comprises communications between control centres, which are necessary for database synchronisation, coordination, cross-data platform access, status reporting, and outage management [13]. These communications may utilise both dedicated private networks and connections through public telecom service providers. Throughput and latency requirements vary depending on the applications [13].

The inter-control centre protocol (ICCP) assures these communication services. It defines requirements governing how utilities control centres communicate with each other over a wide area network (WAN) and it is standardised by IEC 60870-6 [13], [15], [16].

2.1.4 Distribution grid automation and customer communications

This area is seeing rapidly emerging communications applications, emphasizing the changing nature of the electric power grid that is expected to accelerate with the coming smart grid paradigm [4].

Distribution automation includes supervision and control, FDIR (fault detect, isolate and service restore), and Volt-VAR control (capacitor bank and tap changer commands) [13].

The emerging applications in the customer space include smart metering, demand response, and the possibility of controlling of distributed power generators residing at the customers' residences. The applications require two-way communications from and to the grid.

Metering services may use public communication services, but distribution automation, with its high service requirement, still require dedicated communication services.

Smart metering is standardised by IEC 62056-31, which superseded IEC 61107 [16] [3].

2.2 Smart grid communications

2.2.1 Overview

As previously discussed, the smart grid will be full of sensors, actuators, and controls providing real-time full situational awareness and automation of the entire grid, including customer's premises. To realise the benefits from these communications services, a new extended communications network architecture is needed [4]. Therefore, the electric grid will require an integrated communications network, spanning the generation, transmission, and distribution segments.

This multi-tier communications network will be flexible and easily extendable to allow for control and reliable operation of a grid capable of bi-directional flow of electrical energy.

The network has three main components including the home area network (HAN), neighbourhood area network (NAN), and wide area network (WAN) [4].

2.2.2 Home area network (HAN)

This network, in the smart grid (SG), will connect all household electrical devices with the gateway or home meter and will provide advanced metering applications. This network will provide access to household appliances and will reside at the customer premises. It would enabling home automation networks perform applications such as smart metering and demand response [17]. Similar networks in businesses are called business/building area network (BAN), while those in industrial settings are referred to as industrial area network (IAN).

With data speeds in the 1-10 kbps range and the requirement for flexibility, wireless communication will preferred in this network [4]. This network can utilise both proprietary and open wireless protocols such as IEEE 802.15.4, Z-Wave and IEEE 802.11, or alternatively) HomePlug through powerline communications (PLC) [4].

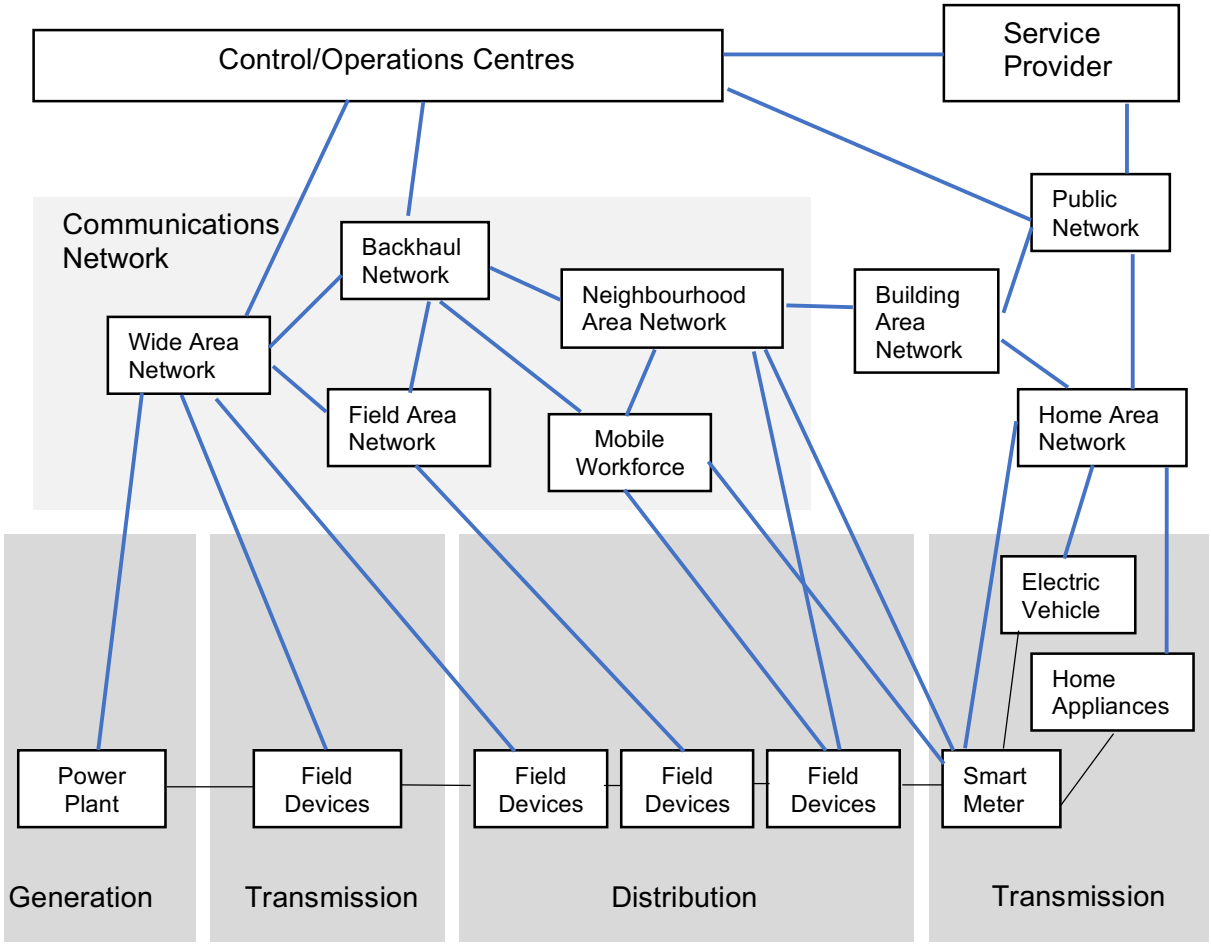

Figure 2.1 Extended communications network for the smart grid [4]

2.2.3 Neighbourhood area network (NAN)

This network will link several smart home meters (from the home area networks) together, providing connectivity to local access points. It is called a field area network (FAN) when it is deployed for data collection in grid monitoring applications.

NAN would have data rates of around 10 -1000 kbps, and would utilise both wireless and wired technologies [4], as shown in Table 2.2.

2.2.4 Wide area network (WAN)

This network would have the widest coverage and highest data rates, typically around 10-100 Mbps. Core utility systems and the grid will be connected through the WAN. It would link the

core network to the NAN (the Backhaul Network) and also utility and substations to metro networks (Core Network) [4].

The backhaul network may use wireless technologies described above for the NAN, while the core network may utilise fibre (SONET), Internet Protocol/Multiprotocol Label switching (IP/MPLS), and similar wired technologies [4], [17].

Table 2.2 Connectivity options for smart grid communications network [18]

Corporate networks	To grid assets (typically dedicated links)	Access WAN (FAN and NAN)	Within the home (HAN)
Ethernet Private circuits	Wireless 2G/3G/4G Wireless dedicated spectrum Fibre optic Satellite Leased line	Wireless/Mobile/GPRS Long-rang radio RF mesh Fibre optic Broadband PLC WiMAX/LTE	Wi-Fi Z-wave ZigBee HomePlug

2.3 Co-simulation of power system and communication network

Innovative features such as automation, bi-directional power flow, and full situational awareness of the grid that will be achievable with a smarter grid will rely largely on information and communication technology [1].

As these communication networks become more pervasive, and the volume and instances of information flow in the grid increases, the cyber-physical interactions between the communication and power systems become more critical. Simulation offers a cost effective and safe way to study this interaction and to assess the effects the communication systems may have on the electric grid's performance.

Open source and commercial simulation tools exist for modelling and analysing the power systems and communication domains separately. But as communication becomes increasingly important to the operation of the grid, it is advantageous to study them together, hence the need for co-simulation of both domains.

In the literature, integrated, offline, and real-time simulations have been proposed as solutions to the co-simulation of both domains [19], [20].

2.3.1 Real-time co-simulation

Here, the simulation clock is synchronised with the time in the real world. That is, the physical system and the computer model run at the same rate. For real-time simulation, data is exchanged in real time between the communication and power system modules [19].

This simulation method does not encounter data exchange and time synchronisation issues, but the cost of setup is a disadvantage. Additionally, it is difficult to test what-if scenarios due to the length of simulation time in this method [21].

An example of work in this area is [22], which couples a commercial communication simulator ns-2 (Network Simulator version 2) with the PSS® NETOMAC (Power System Simulator and Network Torsion Machine Control), which is a mathematical solver within the Siemen's commercial power system simulation software PSS®, to model the power system. This work concentrates on (soft) real-time simulation. Other works in this area include [15] and [16].

Table 2.3 Examples of power system and communication simulators [20]

Power system		**Communication system**	
Simulation tool	License	Simulation tool	License
Cymdist		Network Simulator (ns2 and ns-3)	Open source
DIgSilent	Commercial	OMNeT++	Open source
EMTP-RV	Commercial	NeSSi	Open source
ETAP PSMS	Commercial	OPNET Modeler®	Commercial
EuroStag	Commercial		
homer	Commercial and open source		
ObjectStab	Open source		
OpenDSS	Open source		
PowerWorld			
PSCAD/EMTDC	Commercial		
PSS®E	Commercial		
PSS®Sincal	Commercial		
MATLAB's SimPowerSystems	Commercial		

2.3.2 Offline co-simulation

This method involves combining full-featured power system and communication simulators in their individual domains using data exchange and time synchronisation techniques to produce

models whose simulation clocks run at rates faster than real-time clocks. This method maintains comprehensiveness while providing the flexibility of running what-if analyses [20].

Typical architectures in this method include dedicated synchronisation and control mode and master-slave mode [19]. In the master-slave mode, simulation control logic is entirely implemented in one simulator, called the master. The slave simulator is called only when required by the master simulator, and the two cannot perform tasks in parallel. For the dedicated synchronisation and control mode, the data to be exchange between the simulators are stored in an independent component, which results in the need for synchronisation.

The major drawback of this method is the data exchange and time synchronisation issue. The need for synchronisation adds programming complexity and introduces a performance penalty ([25] shows that simulation overload can account for as much as 90% of the simulation time).

In [26], Positive Sequence Load Flow Analysis (PSLF) software and Power System Computer Aided Design/Electromagnetic Transients including DC (PSCAD/EMTDC) for simulating the power system was combined with ns-2 for the communication network simulation, while authors in [27] combine the Open Distribution System Simulator (OpenDSS) for electrical network simulation with ns-2. Distribution feeders with networked volt/var optimisation were analysed using Offline simulation in [28].

2.3.3 Integrated simulation

In this method, a hybrid system model of the communication and power systems are set up in a single simulation tool [21], [29].

[21] uses Objective Modular Network Testbed simulator (OMNeT++) as the simulation tool. Here, the communication model is readily modelled in OMNeT++ with the electrical network added as modules. The electrical models are basic, however, and the tool is unable to comprehensively simulate the dynamics of the power system.

2.3.4 Analytical alternatives to time domain co-simulation

In analytical approaches, communication time delays (and other sources of time delays) are accounted for by including time delays in the classical hybrid differential algebraic equations (DAEs) that describe the behaviour of the power system, leading to the formulation of delay differential algebraic equations (DDAEs) [30], [31]. The stability of the resulting DDAEs are then analysed analytically.

Reference [30] has analysed the small-signal stability of the DDAEs through its spectral analysis, by transforming the DDAEs into an equivalent partial differential equation. This method like other frequency-domain methods, however, cannot handle uncertainties without difficulty [30]. In [32], a probabilistic approach is used to analyse the effect of PMU

measurement delays on the power system small-signal stability. However, the method is difficult to use for large scale multi-machine power systems and is largely limited to analysing a single machine connected to an infinite bus system [30].

The Lyapunov stability methods have been applied to the stability analysis of time delayed power system in [33] and [34]. However, the Lyapunov based methods only give sufficient conditions for stability [31]. Hence, failure in meeting the conditions does not necessarily imply instability [30], [31]. Additionally, it is difficult to define the Lyapunov functions [35], restricting them to use in small power systems [30].

2.5 Current work

This project uses the integrated simulation method by modelling the power and communication systems in a single tool, using MATLAB/Simulink. It is capable of offline simulation and the problems of data exchange and time synchronisation are absent. Also, MATLAB's power system simulation provides the necessary comprehensiveness needed to study the short- and long-term dynamics of the power grid.

Chapter 3
Modelling and Analysis

3.1 Power system modelling

An equivalent representative Great Britain network (RGBN) like system [10], [11] was modelled in this work to investigate the interactions in the cyber-physical system. This is will allow more realistic dynamic power system responses to be realised and studied.

However, because of the simplifications that were made in this reduced model [10], the results obtained should not necessarily be regarded as accurately representing the behaviour of the real full system.

This reduced model, by resembling the full GB network, makes the construction of scenarios and the interpretation of results easier than using arbitrary power system models.

The data for the reference steady-state model is available in [10], [11] and has been checked against data provided by the National Grid Electricity Transmission (NGET) [10]. It provides detailed model data of the 2010 electricity network of GB that anticipates the 2010/11 “average cold spell” (ACS) winter peak demand loading conditions, as well as the planned transfer to meet that demand.

3.1.1 Steady state model

To build up the structure of the model and to validate against the load flow data in [10], a steady state equivalent model is first built up. This includes using voltage sources as generation models, utilising static constant power loads and losses. The reference network model is shown in Figure 3.1 on top of a GB map. This shows the corresponding locations of the nodes and transmission lines.

The model consists of 29 nodes, which are interconnected through ninety-nine transmission lines in total. Ninety-eight of those are in double circuit configuration, with two transmission lines connecting a pair of nodes. Nodes 2 and 3, however, are connected by a single transmission line. Only positive phase sequence data were given for the network branches. These network branches represent the main routes through which power flows through the actual Great Britain transmission system [10]. Winter post-fault thermal ratings are also given in [10].

Areas in England are represented by twenty-five 400 kV nodes, while those in Scotland are represented by three nodes having a nominal voltage of 275 kV and one node having a

nominal voltage of 132 kV [10]. Transmission lines between two buses with different voltage levels are considered to operate at the voltage level of the higher bus, with a total of eleven transformers connecting the nodes not operating at the same voltage levels [11], [36].

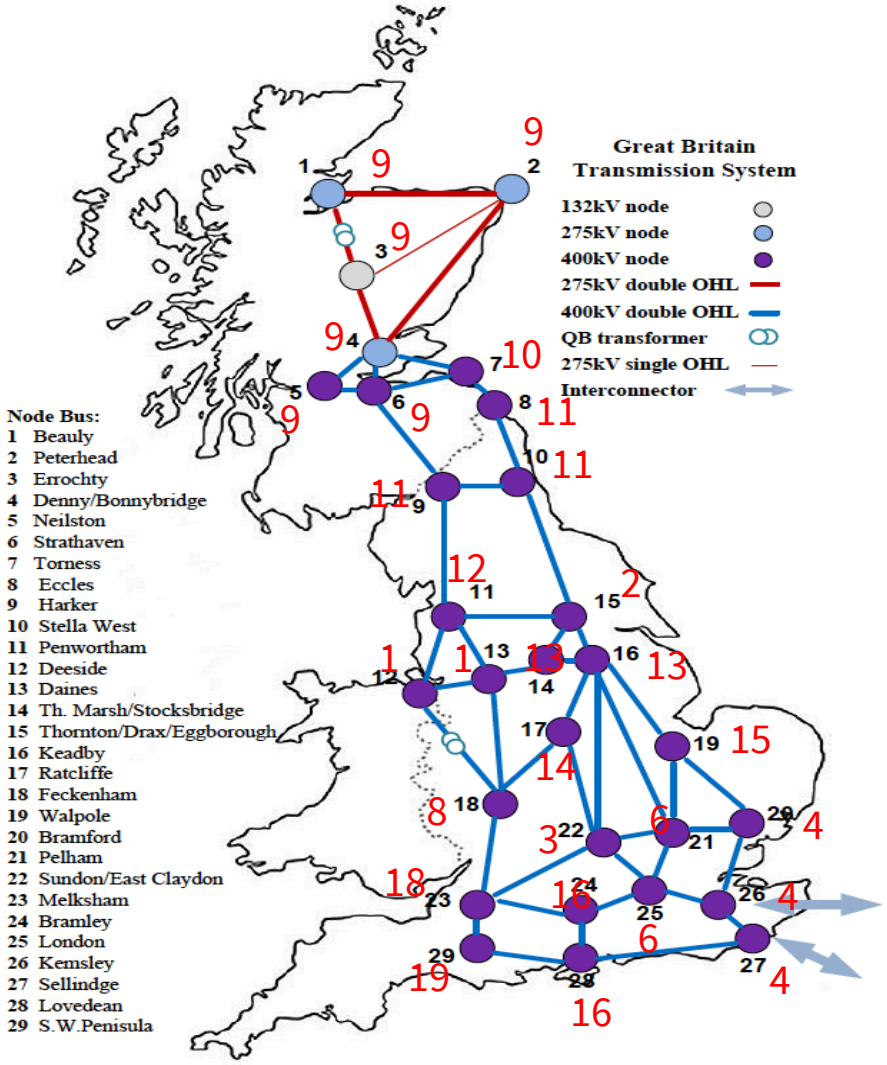

Figure 3.1 Representative GB network model overview (extracted from [36])

The model includes all the main groups of generation in the 2010/11 SYS 'generation background' at the appropriate locations [37], as well as all the groups of demand that were anticipated at 2010/11 "ACS" winter peak demand conditions.

Interconnections with external subsystems are modelled as constant power loads as in [10]. The link from south west Scotland to Northern Ireland is not shown in Figure 3.1.

A total of 24 nodes contain generators. The active power for every node were calculated using the generation scenario in the 2010/11 'SYS background' [10]. Appropriate reactive power

capabilities at specified locations are used in the reduced model to represent the switched reactive compensators in the actual Great Britain network [10].

3.1.2 Power system dynamic model

To explore the system stability, the steady-state model, implemented with data provided in [10], [11], was modified to include dynamic models of loads, generators (together with their controls), a power system stabilizer (PSS) together with a wide area controller. However, it was only possible to model balanced faults as only positive phase sequence data were provided in the reference case [10].

This section describes the dynamic models for the generators (with the corresponding excitation and governing systems), loads, and power system stabilizer.

Synchronous Generator model

Synchronous generators are very important to power systems as they produce the bulk of the electric power [38]. They are also important to the stability of power systems as ensuring that synchronous generators do not lose synchronism with each other is critical to the stable and secure operation of the world's power systems [39].

Hence, the models of the synchronous generating units, along with their controls, are key components to include in the dynamic power system model. However, as actual generation dynamic data were not provided in the reference RGBN model [10], standard or typical data were used in the model implementation.

All convention generators were modelled using detailed sixth-order state-space synchronous generator models.

Full derivation and extensive analysis can be found in [40]. Only key equations are shown here.

The damper windings, field, and stator dynamics are accounted for by the model [40], [41]. The reference frame for the two-axis equivalent circuit is the rotor's, with the electrical variables referred to the stator and indicated with primes [40], [41]. The equations characterising the model are given below [40].

$$v_{qs}^{r} = \omega_r \lambda_{ds}^{r} + r_s i_{qs}^{r} + \frac{d\lambda_{qs}^{r}}{dt} \tag{3.1}$$

$$v_{ds}^{r} = -\omega_r \lambda_{qs}^{r} + r_s i_{ds}^{r} + \frac{d\lambda_{ds}^{r}}{dt} \tag{3.2}$$

$$v_{kq1}^{\prime r} = r_{kq1}^{\prime} i_{kq1}^{\prime r} + \frac{d\lambda_{kq1}^{\prime r}}{dt} \tag{3.3}$$

$$v'^{r}_{kq2} = r'_{kq2} i'^{r}_{kq2} + \frac{d\lambda'^{r}_{kq2}}{dt} \tag{3.4}$$

$$v'^{r}_{fd} = r'_{fd} i'^{r}_{fd} + \frac{d\lambda'^{r}_{fd}}{dt} \tag{3.5}$$

$$v'^{r}_{kd} = r'_{kd} i'^{r}_{kd} + \frac{d\lambda'^{r}_{kd}}{dt} \tag{3.6}$$

The expressions for the flux linkages are shown below.

$$\lambda^{r}_{qs} = L_{ls} i^{r}_{qs} + L_{mq}(i'^{r}_{kq1} + i^{r}_{qs} + i'^{r}_{kq2}) \tag{3.7}$$

$$\lambda^{r}_{ds} = L_{ls} i^{r}_{ds} + L_{md}(i^{r}_{ds} + i'^{r}_{fd} + i'^{r}_{kd}) \tag{3.8}$$

$$\lambda'^{r}_{kq1} = L'_{lkq1} i'^{r}_{kq1} + L_{mq}(i^{r}_{qs} + i'^{r}_{kq1} + i'^{r}_{kq2}) \tag{3.9}$$

$$\lambda'^{r}_{kq2} = L'_{lkq2} i'^{r}_{kq2} + L_{mq}(i^{r}_{qs} + i'^{r}_{kq1} + i'^{r}_{kq2}) \tag{3.10}$$

$$\lambda'^{r}_{fd} = L'_{lfd} i'^{r}_{fd} + L_{md}(i^{r}_{ds} + i'^{r}_{fd} + i'^{r}_{kd}) \tag{3.11}$$

$$\lambda'^{r}_{kd} = L'_{lkd} i'^{r}_{kd} + L_{md}(i'^{r}_{fd} + i^{r}_{ds} + i'^{r}_{kd}) \tag{3.12}$$

where the subscripts are given as:

f	Field winding quantity
k	Damper winding quantity
r	Rotor quantity
s	Stator quantity
d	Direct axis quantity
q	Quadrature axis quantity
l	Leakage inductance
m	Magnetizing inductance

And the variables as:

v	Voltage
r	Resistance
i	Current
ω_r	Rotor speed
λ	Mutual flux
L	Inductance

The equivalent circuit model is shown in the figure below.

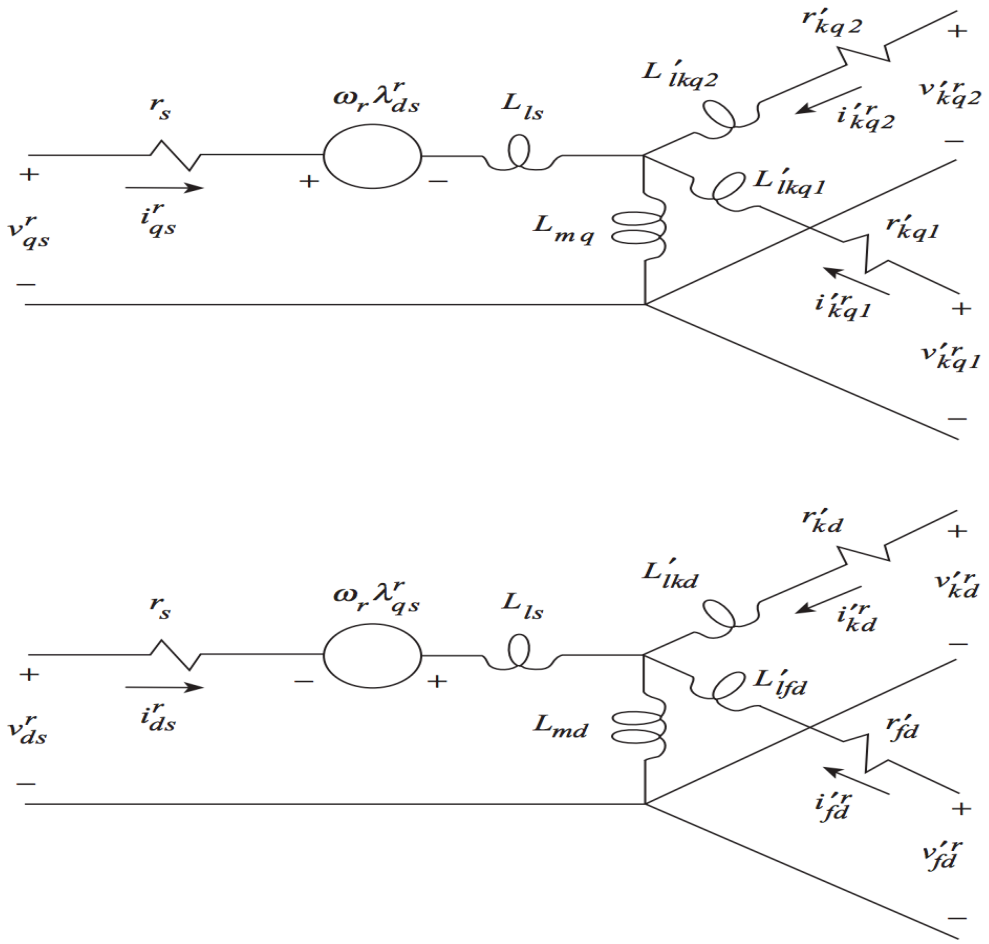

Figure 3.2 Electrical model of three-phase synchronous machine [40]

Similarly, the equations describing the mechanical systems are given by [40], [41]

$$\dot{\delta} = \Delta\omega \tag{3.13}$$

$$\Delta\omega = \frac{1}{2H}\int_0^t (T_m - T_e)dt - k_D\Delta\omega \tag{3.14}$$

$$\omega = \Delta\omega + \omega_s \tag{3.15}$$

where

ω_s	Synchronous speed
δ	Rotor angle of generator
H	Inertia constant of generator
$\Delta\omega$	Stator deviation of generator with respect to the synchronous speed
T_e	Electromechanical torque
T_m	Mechanical torque
k_D	Damping coefficient
ω	Rotor mechanical speed

Excitation system

The DC voltage required for the creation of magnetic fields on the rotors of synchronous generators are generated by the excitation systems [31], [38]. Typically, the source of power for the DC field voltage determines the excitation dynamics and their classifications or distinctions [31], [42].

This work uses the IEEE ST1A excitation system with standard recommended parameters [43]. In this static excitation system, the power for the excitation is gotten from the generator terminals, and is supplied through a transformer and a controlled thyristor rectifier [31]. At its core, the ST1A is made up of a transformer, rectifier, and voltage regulator [31]. The generator terminal voltage is regulated by adjusting the DC output of the thyristor rectifiers [31].

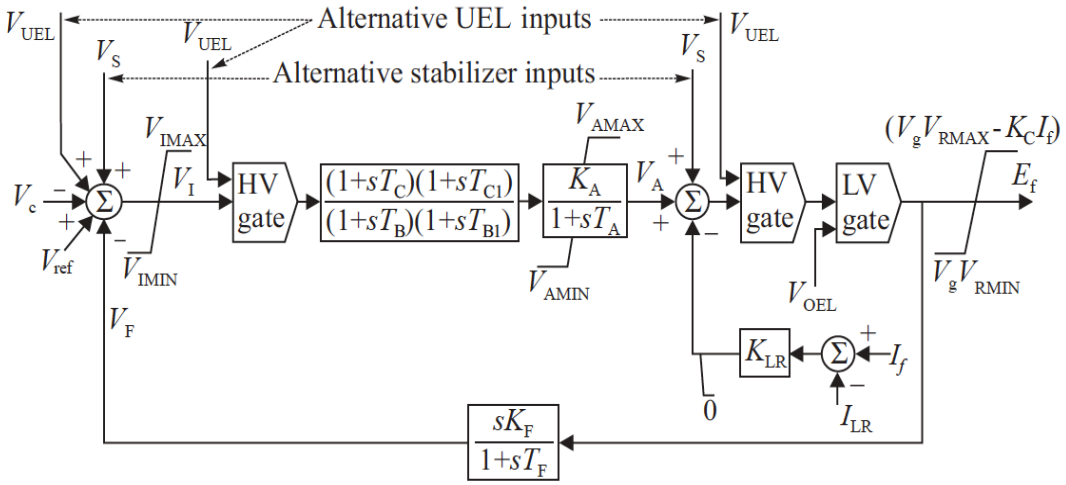

Figure 3.3 The ST1A excitation system [43]

In Figure 3.3, V_{ref} is the reference voltage input and V_c is the generator terminal voltage. V_s represents the auxiliary control reference input for stabilising the system that is obtained from the outputs of the local PSS or wide area damping controller. V_{UEL} is the output signal from the underexcitation limiter. (Due to stability and thermal limits, the reactive power absorbed or injected by the generator is limited by the voltage control [31].)

Turbine Governors

The governor and hydraulic turbine model consisting of a nonlinear hydraulic turbine model, a governor system based on a proportional-integral-derivative (PID) action, and a servomotor described in [44], [45] were used for the hydro plants. For the coal, nuclear, and CCGT plants, a steam turbine and governor system model described in [46], [47] were used.

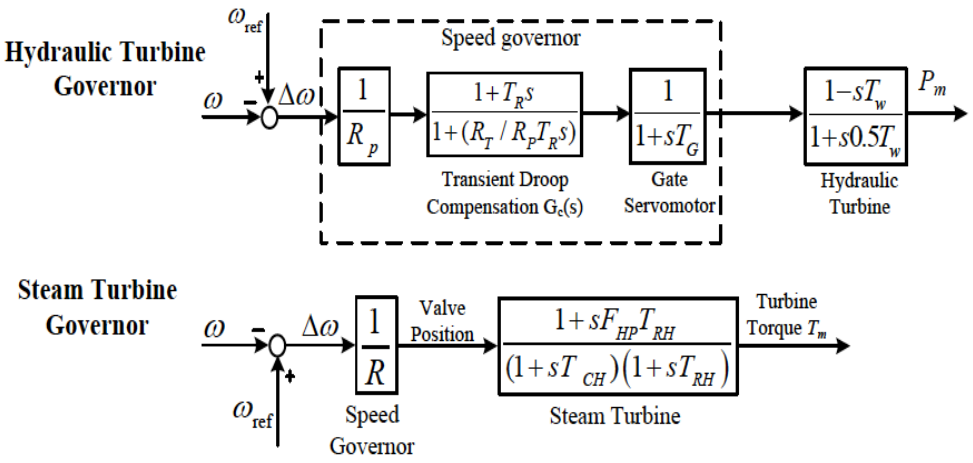

Figure 3.4 Simplified representation of typical models of turbines and their governing systems

Dynamic loads

Dynamic loads' reactive and active powers vary with its terminal voltage. If the load terminal voltage is lower than a predefined value, the impedance of the load is kept constant. Otherwise, it is as governed by the relation given below [48]:

$$\mathrm{P}(s) = P_o(\frac{V}{V_o})^{n_p}\frac{1+T_{p1}s}{1+T_{p2}s} \tag{3.16}$$

$$\mathrm{Q}(s) = Q_o(\frac{V}{V_o})^{n_q}\frac{1+T_{q1}s}{1+T_{q2}s} \tag{3.17}$$

where V_o, P_o, and Q_o represent the initial voltage, active power and reactive power respectively. The instantaneous voltage is given by V. The nature of the load and the reactive and active power dynamics are controlled by n_p, n_q, T_{q1} and T_{q2}, T_{p1} and T_{p2} respectively as shown in Table 3.1.

Table 3.1 Static load representation [48]

Static Load Models	Description	Parameters
Constant impedance (Z)	Power varies directly with the square of the voltage magnitude	$n_p = n_q = 2$ $T_{p1} = T_{p2} = T_{q1} = T_{p2} = 0$
Constant current (I)	Power varies directly with the voltage magnitude	$n_p = n_q = 1$ $T_{p1} = T_{p2} = T_{q1} = T_{p2} = 0$
Constant power (P)	Power does not vary with changes in voltage magnitude	$n_p = n_q = 0$ $T_{p1} = T_{p2} = T_{q1} = T_{p2} = 0$

Power system stabilizer

A Power system stabilizers damps rotor oscillations in power systems by providing supplementary control signal(s) used in regulating the voltage reference input of a generator's automatic voltage regulator (AVR) [49], [50].

A PSS is typically structured as shown in Figure 3.4 [50].

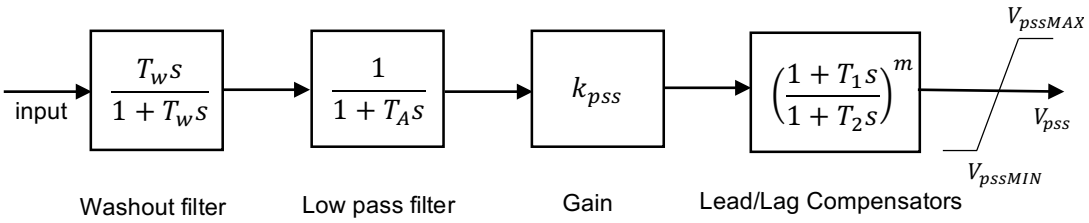

Figure 3.5 Typical PSS structure

The washout filter is needed to minimise changes in generator terminal voltage from the voltage reference during slow frequency changes in the steady state [49]. The low pass filter attenuates high frequency signal components (typically torsional modes) while the lead/lag blocks provide the required phase compensation [36], [49]. The PSS output is limited to prevent it from unduly affecting the AVR's actions [50].

The PSS is conventionally designed and tuned by the P-Vr, Residues, and GEP methods [49]–[51]. In this work, the method of Residues is used and its principles are described briefly below.

Method of Residues

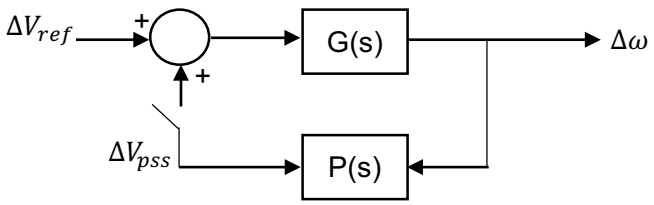

Figure 3.6 Power system and PSS transfer functions on open loop

$G(s) = \frac{\Delta\omega}{\Delta V_{ref}}$ is the transfer function from the voltage reference input to the speed deviation output of the power system where the PSS is to be installed while the PSS transfer function is given as $P(s) = k_{pss}Q(s)$.

The closed loop transfer function of the system is

$$T(s) = \frac{G(s)}{1 - k_{pss}G(s)P(s)} \tag{3.18}$$

If the mode (or eigenvalue) to be shifted to the left is λ_c, the open loop transfer function of the power system when excited by λ_c is given as [49]

$$G(\lambda_c) = \frac{R_c}{s - \lambda_c} \tag{3.19}$$

where R_c is the residue of the eigenvalue λ_c of $G(\lambda_c)$. Detailed derivation of the residues from state equations can be found in [49] and [52].

Substituting (3.19) into the characteristic equation of (3.18), we get

$$s = \lambda_c + k_{pss} R_c P(\lambda_c) \tag{3.20}$$

For a small shift $\Delta\lambda_c$ in the mode of the closed loop system, it can be shown that (3.20), from [49], reduces to

$$\Delta\lambda_c \approx k_{pss} R_c P(\lambda_c) \tag{3.21}$$

For a direct shift of the mode λ_c to the left [49]

$$arg\{R_c P(\lambda_c)\} = \pm 180° \tag{3.22}$$

Therefore, depending on the angle of the residue, the time constants of the lead/lag compensators are designed to provide phase lead or phase lag compensation to ensure (3.22) is satisfied [49].

Dynamic system implementation

The generators were implemented in Simulink with the help of component libraries from Simscape Power Systems [53]. Active and reactive power data along with other generation data were obtained from [10], [11] and the different generator types were parameterised with the corresponding data recommended in [54]. The conventional generator types were represented by hydro (pumped storages were represented with hydro dynamic parameters), nuclear, coal, and combine cycle gas turbine (CCGT) while the intermittent renewable generation were represented by wind turbine generators.

In all, 43 synchronous generators and 7 Type 1 [55] wind generation plants, modelled with asynchronous generators, were added to the power system model.

The IEEE standard ST1A excitation system [43] was used for each synchronous generator.

Figure 3.7 shows the Simulink implementation of the generators at the Beauly node. The other 23 nodes with generation where similarly implemented.

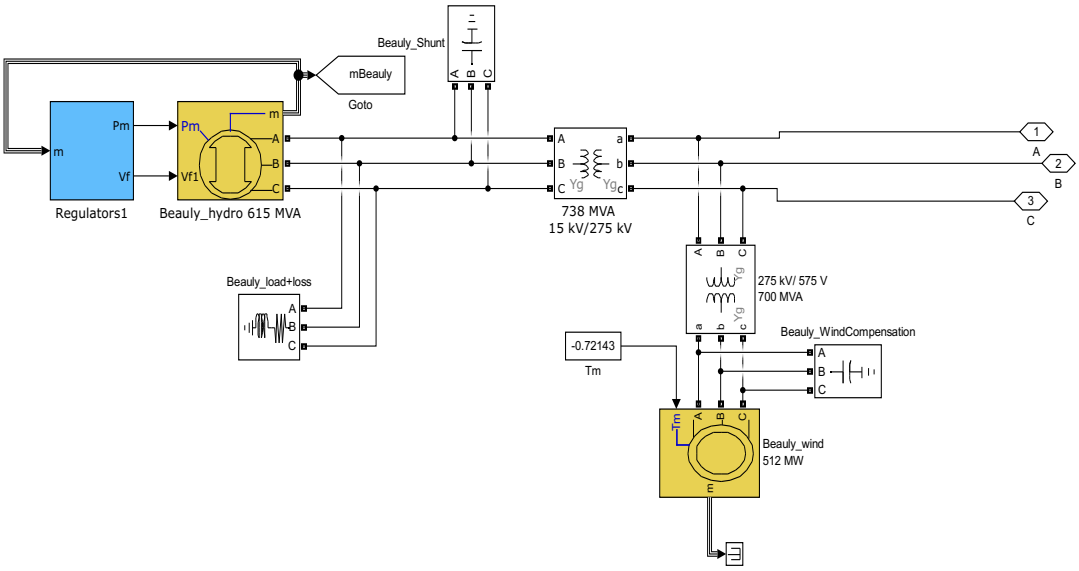

Figure 3.7 Simulink implementation of the generators at the Beauly node

The regulators subsystem contains the synchronous generators controls – comprising the excitation system and governors. The generators are connected to the high voltage network by appropriate transformers.

Besides the installed switched shunt devices at each node, additional reactive power compensation was added to compensate for the reactive absorbed by the asynchronous generators. The SVC reactive power compensation from the reference load flow [10] were replaced with static reactive power compensation.

Details of the generator parameters used are given in Appendix A1.4.

3.2 Communication system modelling

Optical fibre is chosen as the communication channel for this project. This section details the modelling of the fibre optic channel and the communication topology implemented.

3.2.1 Fibre optic modelling

The mathematical basis for understanding optical fibres propagation characteristics are usually the equations by Maxwell [56].

$$\frac{\partial \mathbf{D}}{\partial t} = \nabla \times \mathbf{H} \tag{3.23}$$

$$\frac{\partial \mathbf{H}}{\partial \mathrm{t}} = \frac{1}{\mu_o} \nabla \times \mathbf{E} \tag{3.24}$$

$$\mathbf{D} = \varepsilon_o \mathbf{E} + \mathbf{P_L} + \mathbf{P_{NL}} \tag{3.25}$$

where $\mathbf{P_L}$ is the linear part of the induced polarisation and $\mathbf{P_{NL}}$ the non-linear part. They model the effects of the fibre material on the signals being propagated [56].

Typically, network simulation tools, as a result of computational constraint, use the Nonlinear Schrödinger's Equation (NLSE) to approximately represent the full rigorous model [56].

The NLSE is given by [57]:

$$\begin{aligned} \frac{\partial \mathrm{A(z,t)}}{\partial \mathrm{z}} + \frac{\alpha}{2} A(z,t) + \beta_1 \frac{\partial \mathrm{A(z,t)}}{\partial \mathrm{t}} + \frac{j}{2}\beta_2 \frac{\partial^2 \mathrm{A(z,t)}}{\partial \mathrm{t}^2} - \frac{1}{6}\beta_3 \frac{\partial^3 \mathrm{A(z,t)}}{\partial \mathrm{t}^3} \\ = -j\gamma |A(z,t)|^2 A(z,t) \end{aligned} \tag{3.26}$$

where β_1 represents the differential group delay (DGD) and β_2 and β_3 the second- and third-order factors of the group velocity dispersion (GVD). The spatial longitudinal coordinate is indicated by z, while the nonlinear coefficient is accounted for by γ and α represents the attenuation of the fibre [57].

In operator form, (3.26) can be rewritten as [56]:

$$\frac{\partial \mathrm{A(z,T)}}{\partial \mathrm{z}} = \{\hat{L} + \hat{N}\} A(z,T) \tag{3.27}$$

where T stands for t - $\beta_1 z$, $\hat{L}$ the linear operator and $\hat{N}$ represent the nonlinear operator. $\hat{L}$ and $\hat{N}$ assume the following forms:

$$\hat{L} \rightarrow -\frac{j}{2}\beta_2 \frac{\partial^2}{\partial \mathrm{T}^2} + \frac{1}{6}\beta_3 \frac{\partial^3}{\partial \mathrm{T}^3} - \frac{\alpha}{2}; \;\; \hat{N} \rightarrow j\gamma |A|^2 \tag{3.28}$$

A Split-Step integration algorithm, as described in [56], can be used to address the problem.

3.2.2 Communication network topology

The BT 21st century network (BT 21CN) core nodes serve as the communication network topology for the project. This IP over WDM core network [58] (which uses optical fibre as the communication channel) is depicted below:

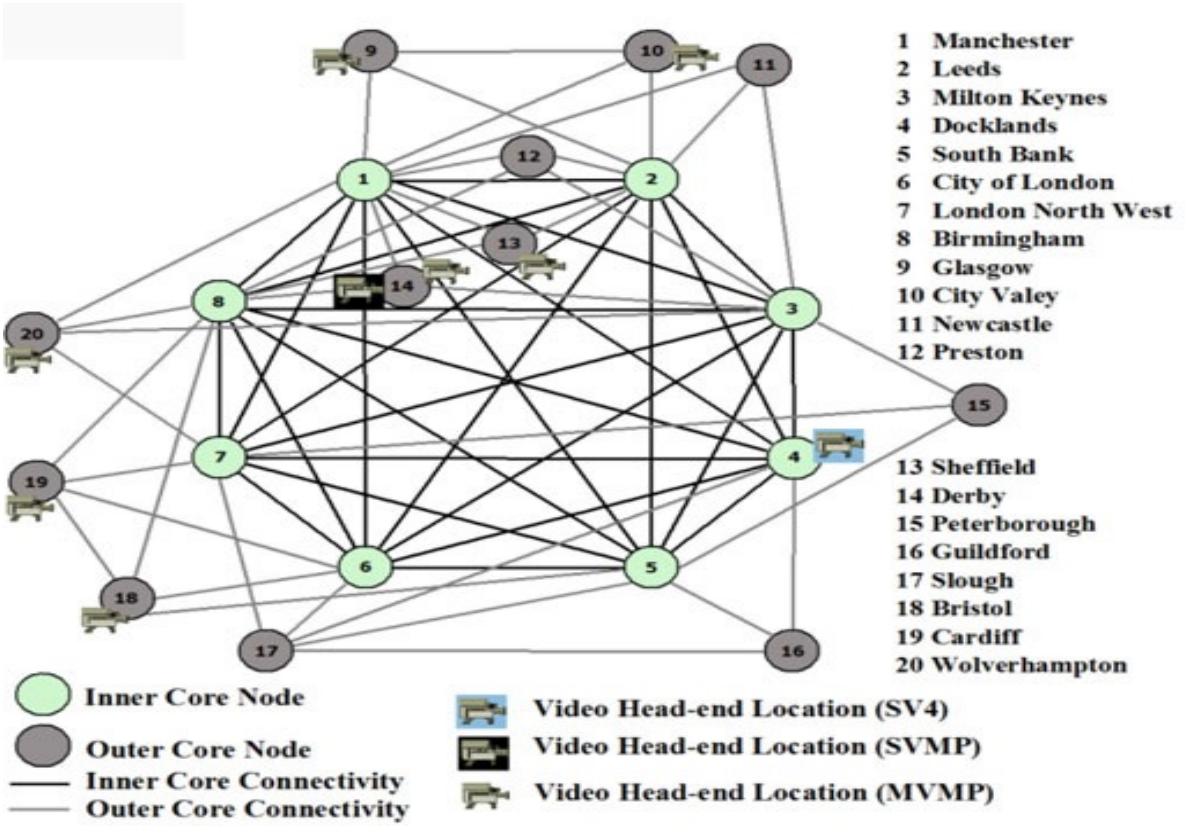

Figure 3.8 The BT (UK) fibre core network (extracted from [12])

In total, there are 20 nodes interconnected by 68 links in this core topology [12]. The core nodes consist of inner and outer core nodes. The eight inner core nodes are fully meshed while the twelve outer nodes are connect with a minimum of 3 other nodes [12].

The relative locations of the power system nodes in the representative GB model with relation to the BT 21CN core nodes are shown in Appendix A.

A MATLAB heuristic function is used to calculate the delay between BT Core network nodes. There exist multiple paths between the core nodes due to the interconnections of the nodes; the function selects the optimum path that minimises the energy consumption of the network components between the two nodes [59].

Direct lightpath bypass MATLAB heuristic function

The direct lightpath bypass involves creating a logical (virtual) link between every network node pair with non-zero traffic demand [59]. The set of all such logical links constitute the virtual topology. For this, the demand data for the nodes is obtained by the function and sorted from each source node to destination node. The sorted demand queue is looped through, and a virtual link is created if there is demand between a sending node and a receiving node. For each virtual link created, the number of wavelengths used, accumulated demand, and available bandwidth are stored.

A physical route for each logical link determined above is then determined. To achieve this, the virtual links are routed over the physical path to minimize the number of network hops and physical distance in order to reduce the time delays. The shortest path problem is solved using the MATLAB '*graphshortestpath*' function from bioinformatics toolbox.

The delays, including propagation and component delays, are then computed. The component delays include the router and switch delay and the delays introduced by the optical transponders and erbium-doped fibre amplifiers (EDFAs). It should be noted that since the aim is to obtain *representative* time delays for a real communication network, the component delays used in the heuristic function are only ball park estimates and may not necessarily represent the actual delays introduced by components in the BT 21CN core network.

The total delay between each network node pair is then stored in an array and made accessible to the physical power system modelled in Simulink.

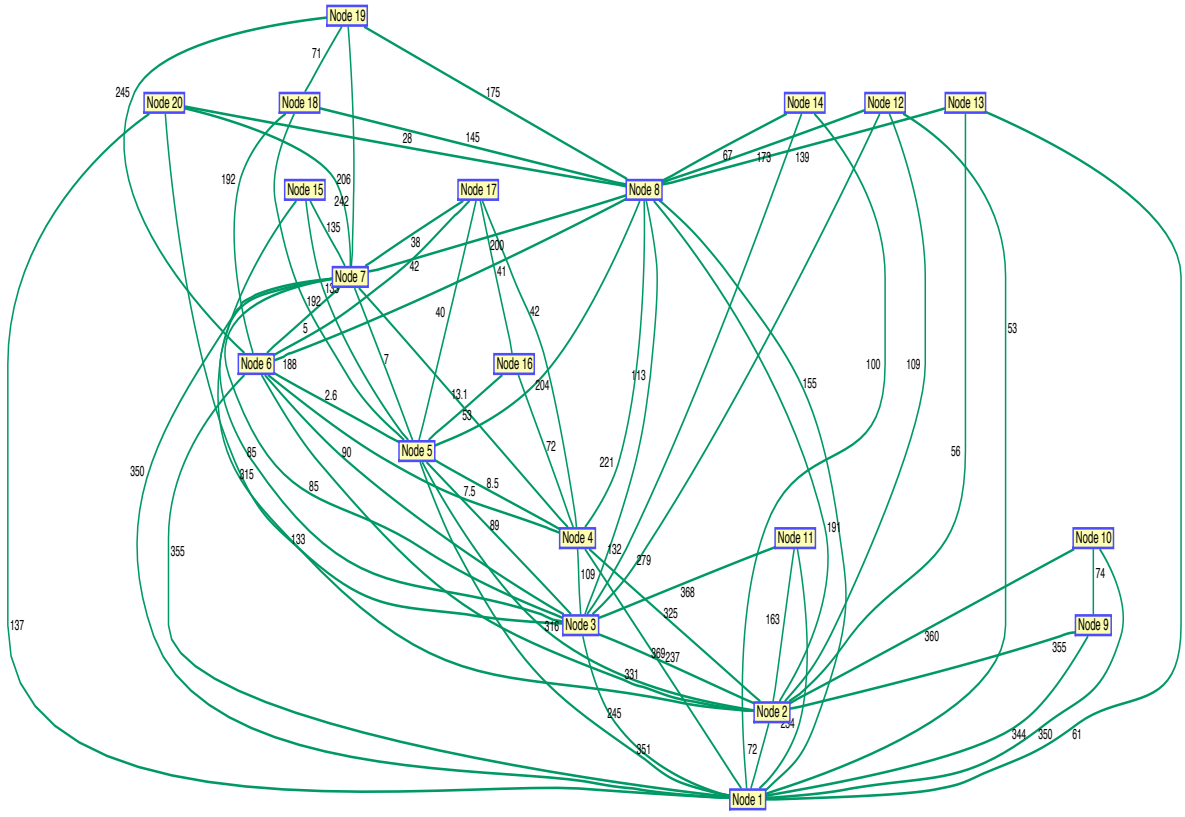

Figure 3.9 Undirected graph of network nodes showing physical distances of fibre links in km

3.3 Wide area damping control

Wide area measurement systems utilising GPS synchronised phasor measurement units (PMUs) can provide power system dynamic data in real time, thereby improving system awareness and making wide area control possible [13], [50], [60].

Power system oscillations, especially inter-area oscillations, can limit the power transferred through tie-lines, thereby increasing economic cost. Moreover, lightly damped or unstable inter-area modes affects the system security and may result in system-wide failures [60], [61]. Wide area damping controllers with stabilising signals having global observation of the inter-area modes, these oscillations can be more effectively damped than using the conventional single input single output (SISO) local power system stabilisers (PSS), which uses local inputs. This is especially true for some cases where inter-area modes may be observable from one area and controllable from a different area [62].

Robust control techniques based on H_∞ methods have been successfully used to design such wide area damping controllers in the literature [50], [60], [63], [64]. This technique is used for this current project. Other techniques include model predictive control and artificial intelligence such as fuzzy logic, genetic algorithm, artificial neural network, and particle swarm [64].

However, due to the large distances involved in wide area control, the communication delay of the links may play an important role, possibly degrading the performance of the wide area damping controller or potentially leading to system instability [65]. Table 3.2 [66] shows the delays associated with several communication links. The remainder of this section discusses the principle of the H_∞ technique that would be used in the wide area damping controller design in this current work.

Table 3.2 Delays associated with several communication links [66]

Communication links	One way delay (ms)
Satellite links	500-700
Fibre optic	100-150
Power line	150-350
Microwave links	100-150
Telephone lines	200-300

3.3.1 Time delay modelling

The Laplace transform of a time delay is expressed as $e^{-s\tau}$ [67]. However, the time delay is usually approximated as a rational polynomial for ease of analysis and simulation [67]. The Padé approximations [68] are most frequently used to approximate the time delay [67]. The higher the order of the Padé approximation, the more accurate the approximation, with a corresponding increase in complexity [69]. In this work, a sixth order Padé approximation to the time delay is used.

3.3.2 $\mathbf{H}_\infty$ control

For a linear system with transfer function E(s), its H_∞ norm is the highest gain of the transfer function over all frequencies input directions [50], [70]. It can be expressed as

$$\|E(s)\|_\infty \triangleq \max_\omega \bar{\sigma}\left(E(j\omega)\right) \tag{3.29}$$

where $\bar{\sigma}(\cdot)$ represents the maximum singular value.

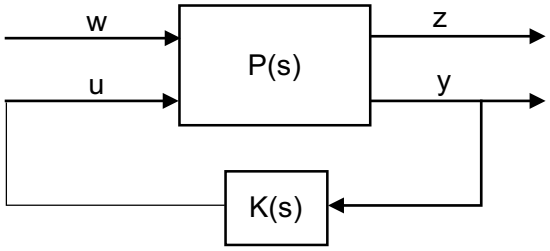

Figure 3.10 Generalised two-port plant diagram

In Figure 3.10, P(s) is the transfer function of the plant and K(s) that of the controller.

Let P(s) have the following realisation [70], [71]

$$\dot{x} = Ax + B_1 w + B_2 u \tag{3.30}$$

$$z = C_1 x + D_{11} w + D_{12} u \tag{3.31}$$

$$y = C_2 x + D_{21} w + D_{22} u \tag{3.32}$$

where w is disturbance vector, x is the state vector , y is the observation vector, z is the error vector, and the control vector is represented as u [71].

The partitioned plant P can be represented as [70], [71]

$$P(s) = \begin{bmatrix} A & B_1 & B_2 \\ C_1 & D_{11} & D_{12} \\ C_2 & D_{21} & D_{22} \end{bmatrix} = \begin{bmatrix} P_{11}(s) & P_{12}(s) \\ P_{21}(s) & P_{22}(s) \end{bmatrix}$$

The closed loop transfer function from w to z is given as [70]

$$T_{wz}(s) = P_{11}(s) + P_{12}(s)K(s)(I - P_{22}(s))^{-1}P_{21}(s) \tag{3.33}$$

The H_∞ problem involves designing a controller that internally stabilises the controlled system and makes

$$\|T_{wz}(s)\|_\infty < \gamma \tag{3.34}$$

for a given scalar γ [50], [70], [71].

3.3.3 Formulation of mixed-sensitivity for $\mathbf{H}_\infty$ control

For control effort optimisation and output disturbance rejection, it is required to design a stabilising controller, K(s), that minimises

$$\left\| \begin{bmatrix} W_1 S \\ W_2 KS \end{bmatrix} \right\|_\infty \tag{3.35}$$

where G(s) is the open loop transfer function of the system to be controlled, the sensitivity $s = (I + GK)^{-1}$ is the transfer function from the disturbance vector w to the observation vector y, and KS measures the control effort [50], [72]. Figure 3.7 illustrates the standard mixed-sensitivity formulation.

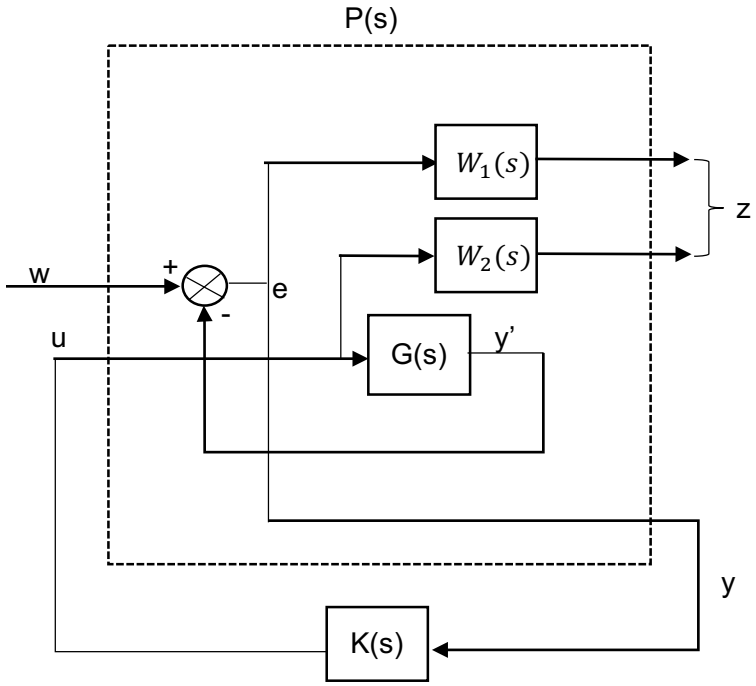

Figure 3.11 Illustration of mixed-sensitivity

For output disturbance rejection, a low-pass filter, W_1, is typically chosen and W_2 is a high-pass filter chosen to minimise the control effort at higher frequencies [50].

The mixed-sensitivity problem is converted into the standard H_∞ problem by computing an augmented plant, P(S), formed from the open loop transfer function and the weighting functions [50].

The solution to the H_∞ problem is to find all the controllers that stabilises the system internally and satisfies Equation 3.34, and it involves solving algebraic Riccati equations [50], [71], [73]. The solution to the Riccati equations can be approached analytically or numerically [50].

The numerical approach involves converting the non-linear Riccati equations into linear matrix inequalities (LMIs), which are computationally easier to deal with [50]. With the LMI approach, the poles of the controlled system can be placed in a specified region on the complex plane

by specifying additional constraints [50], [60]. To assure a minimum damping ratio, the closed loop poles can be placed within a conic sector lying in the left-hand plane having its tip at the origin and with an its inner angle specified in terms of the minimum damping ratio [50].

Additionally, the numerically computed controllers do not have pole-zero cancellations between the controller and plant like their analytical counterparts [50], [74].

Chapter 4

Simulation, Results and Discussion of Results

4.1 Static power system model

4.1.1 Validation of representative GB model

The steady-state equivalent model of RGB network was constructed in MATLAB/Simulink and the load flow results were validated against the reference load flow data in [10].

Due to the inclusion of line transformers, the resulting system's voltage and angle profiles are slightly different from the reference case. However, as can be seen in systems operating point comparison in Appendix A, the developed model is very close to the reference case scenario.

4.1.2 Simulation results from steady-state model

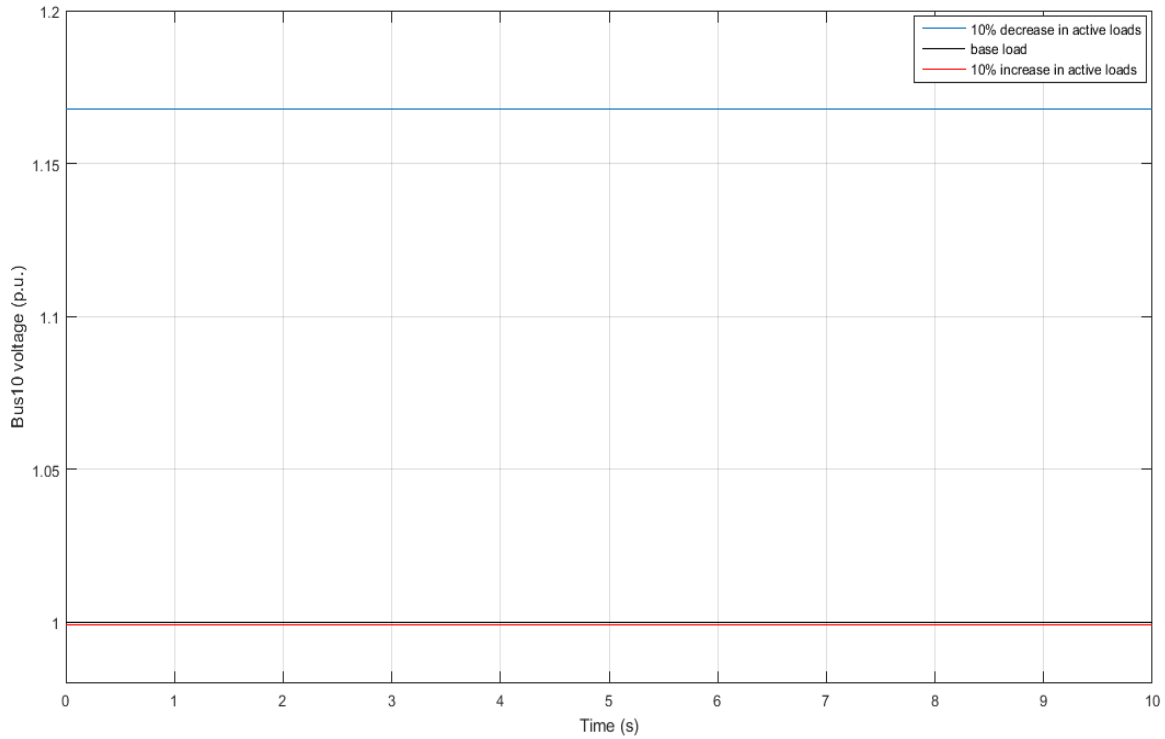

Figure 4.1 Variation in bus voltage with changes in system's loads

Figure 4.1 shows the changes in the per unit voltage when the base load of the system is scaled up or down. With the base load in the reference case, bus 10 is at a voltage of 1.0 per unit of the nominal voltage. A ten percent decrease in the active loads in the system results in a rise in the voltage at bus 10 to 1.168 per unit. On the other hand, a ten percent drop in the active loads reduces the voltage at bus 10 slightly to 0.999 per unit.

Figure 4.2 shows the fluctuations in the voltages of buses 9 and 14 (the buses with the largest deviations from their nominal voltages) when a three-phase-to-ground fault is applied in the system. The three-phase-to-ground fault is applied for 20 cycles before it is cleared.

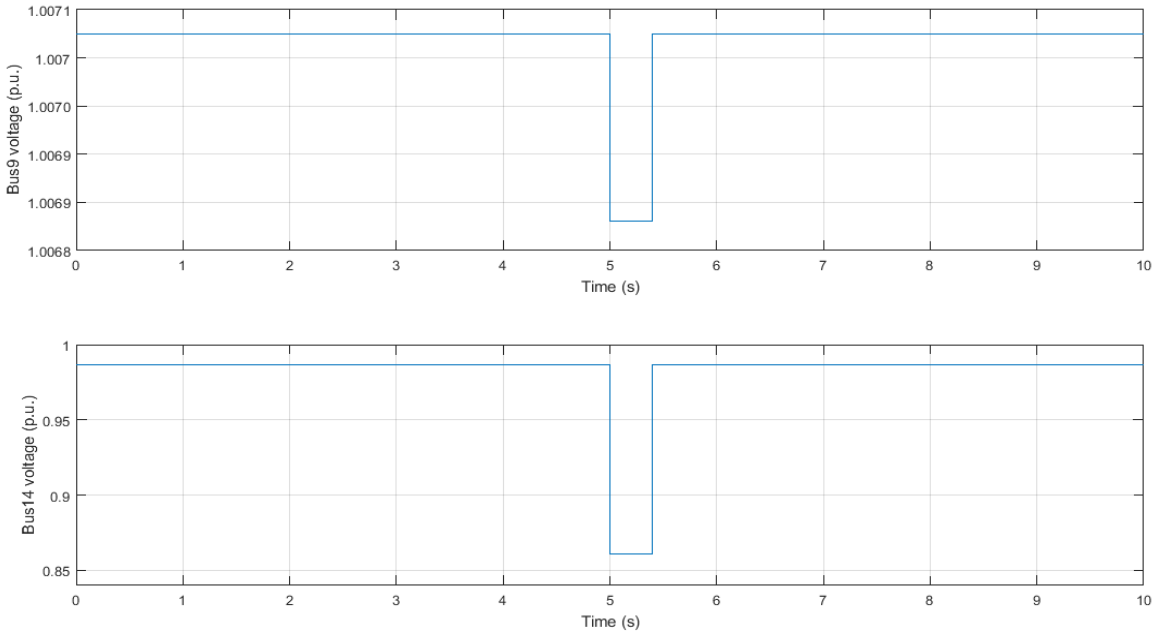

Figure 4.2 Voltage fluctuations of steady-state model following a three-phase-to-ground fault

It is can be observed from Figure 4.1 that the fall and recovery in the voltages are almost instantaneous. This is due to the lack of dynamic data in the modelling of the current system.

4.2 Communication link

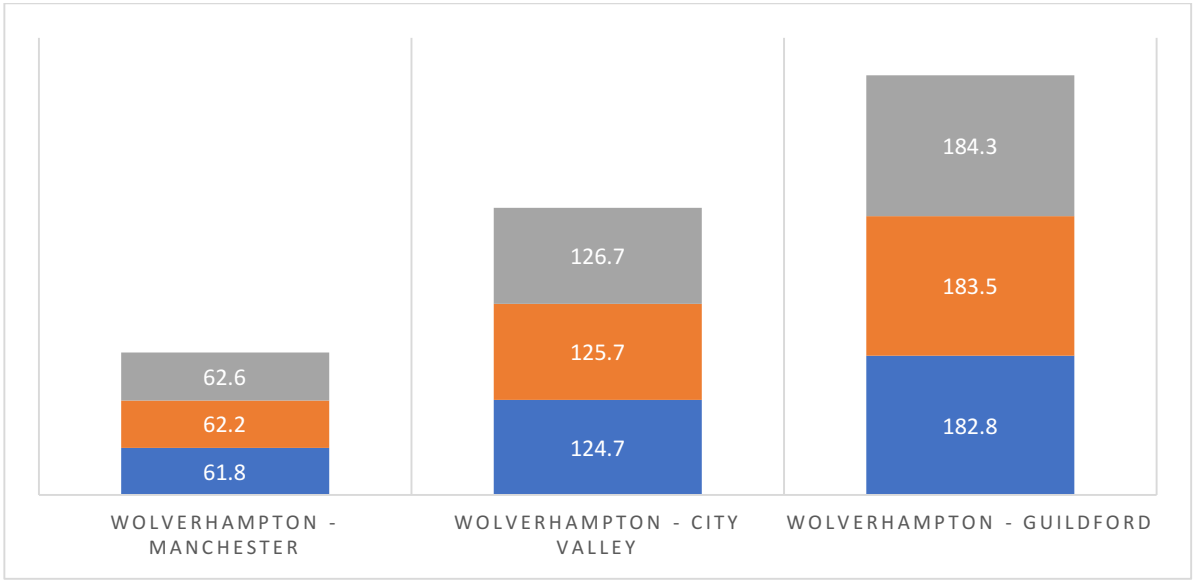

Figure 4.3 Communication link delay in milliseconds

Figure 4.3 is used to illustrate the MATLAB heuristic function that calculates the delay between the UK (BT) Core network nodes described in section 3.

Figure 4.3 shows the delay, in milliseconds, between the core network nodes in Wolverhampton and Manchester, Wolverhampton and City Valley, and Wolverhampton and Guildford with successive increases in the background data by 100 Gbps.

The delay between the nodes at Wolverhampton and Manchester is the shortest of the three because there is a direct link between the two nodes, resulting in a smaller propagation delay.

It can be seen from the figure that the effect of background data is substantially smaller than the effect due to the propagation delay, with an additional 200 Gbps background data increasing the delay by only 0.8 milliseconds.

4.3 Dynamic power system model

After the addition of the dynamic generator models, governors, excitation, automatic voltage regulators, and transformers, the operating point of the system changed slightly. This change was mainly due to changes in reactive power flow owing to the generators' transformer losses and reactive power consumption by the asynchronous generators used in modelling the wind power sources.

As a consequence, appropriate reactive power compensation was added, and the resulting operating point was still very close to the reference case. Appendix A shows the new operating point, with comparisons with the reference case and the static model included.

4.3.1 Eigenvalue analysis

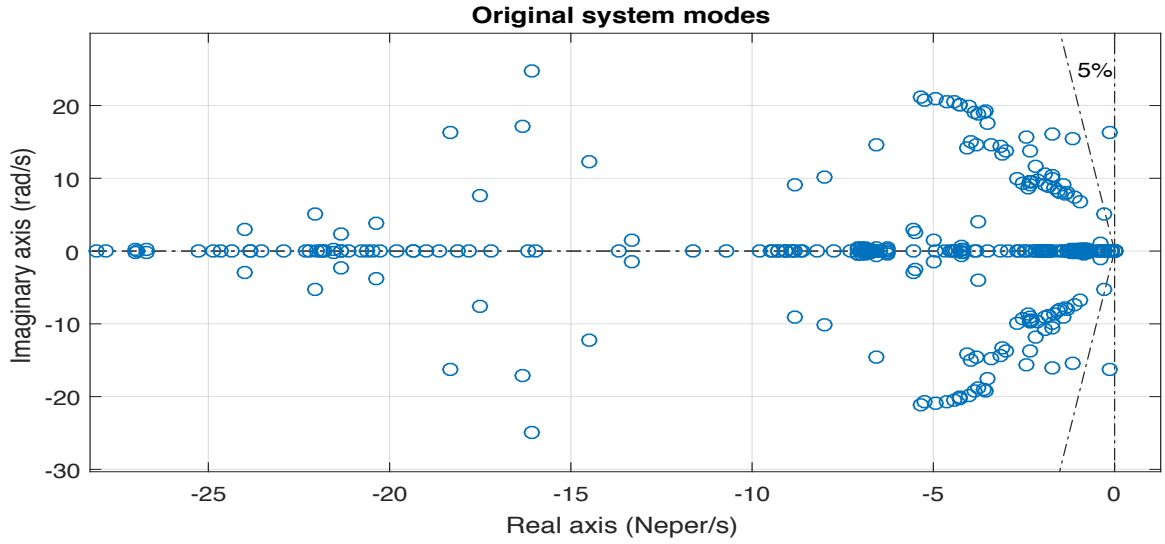

Figure 4.4 Plot of eigenvalues for reference case

To enable eigenvalue analysis, the model was linearized, resulting in a linear model containing 797 states. Figure 4.4 shows the plot of eigenvalues for the reference case load flow data. It can be observed that the real parts of all the eigenvalues lie to the left of the plane, indicating that there are no unstable modes. However, at least one mode is poorly damped, lying outside the five percent damping ratio line.

The zoomed in eigenvalues plot is shown in Figure 4.5 below. This shows the modes with real parts greater than -1.

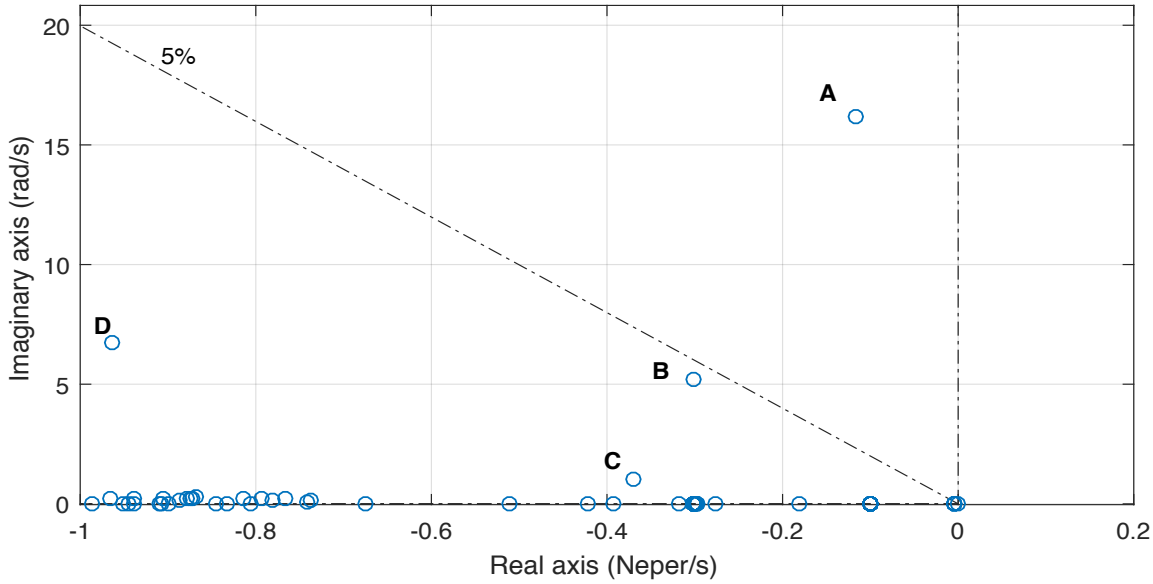

Figure 4.5 System critical modes

From participation factor analysis, it was determined that the four modes were all electro-mechanical modes. Modes C and D are well damped, with damping ratios above 10 %, while mode A has a poor damping ratio of just 0.72 %. Modes A and B are expected to have more significant effects in the system's small-signal response, with their lower damping ratios and slower oscillation decay time. Details about the modes are summarised in the Table 4.1 below.

Table 4.1 Critical modes of reference case

Mode	Eigenvalue	Frequency (Hz)	Damping Ratio (%)	Description
A	$-0.1165 \pm j16.1938$	2.58	0.72	Intra-station mode
B	$-0.3024 \pm j5.1925$	0.83	5.81	Inter-area mode
C	$-0.3699 \pm j1.0082$	0.16	34.44	Global mode
D	$-0.9627 \pm j6.772$	1.08	14.07	Inter-area mode

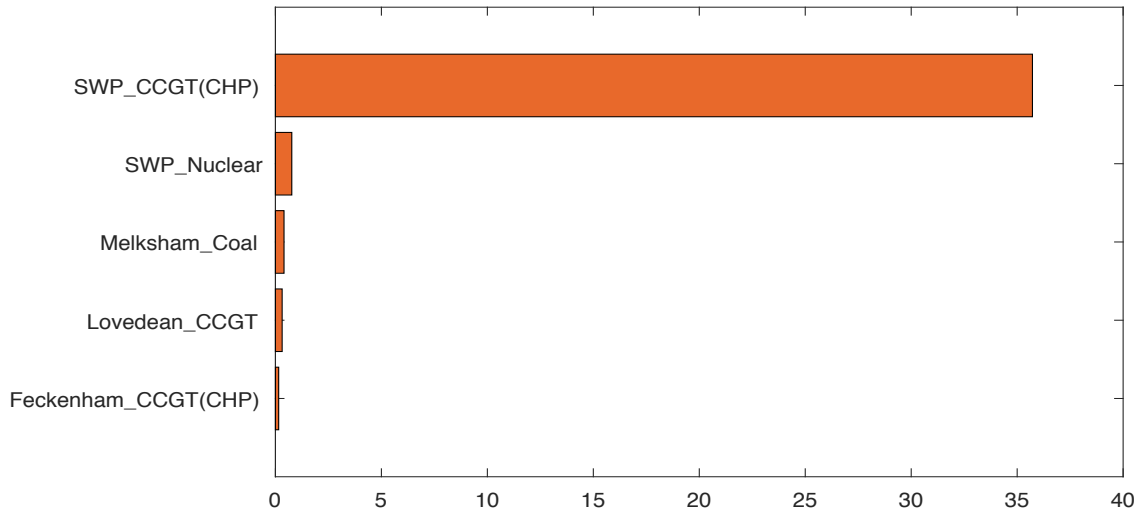

Figure 4.6 Participation factor for mode A

Figure 4.6 shows the participation of the speed deviation states of the generators in mode A, normalised to 100 %.

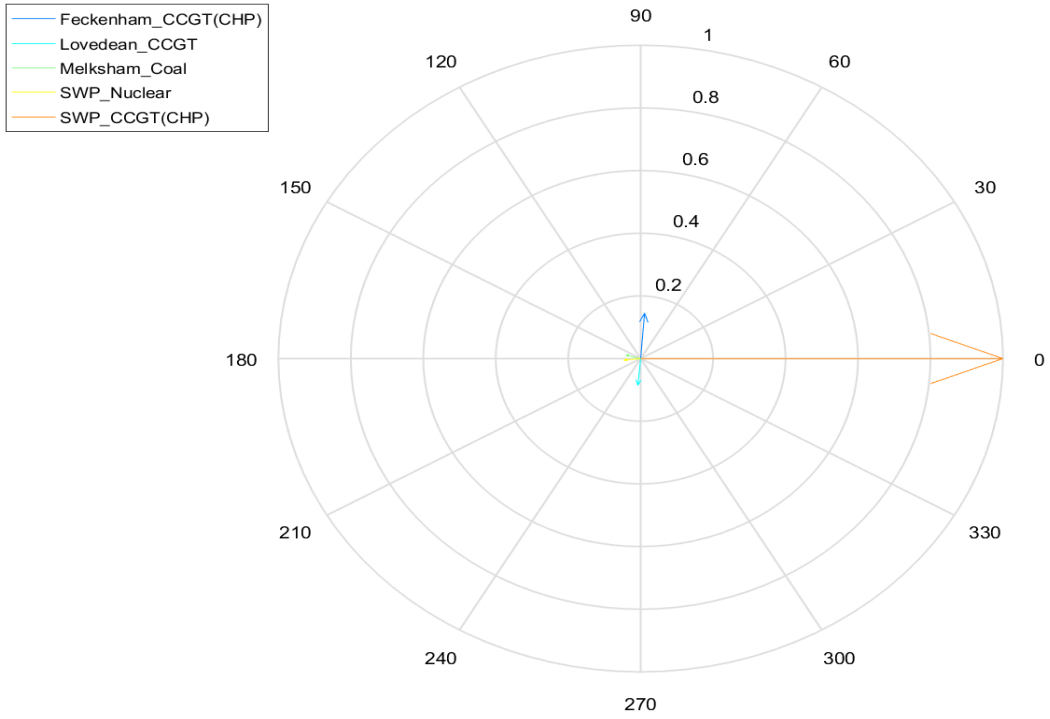

Figure 4.7 Modal shape for mode A

From the mode shape and participation factor, it can be concluded that mode A is an intra-station mode [50], [49], with the two generators at the SWP bus swinging against each other. The Feckenham generator has negligible participation in this mode and can be ignored. The other generators are electrically connected to the SWP bus.

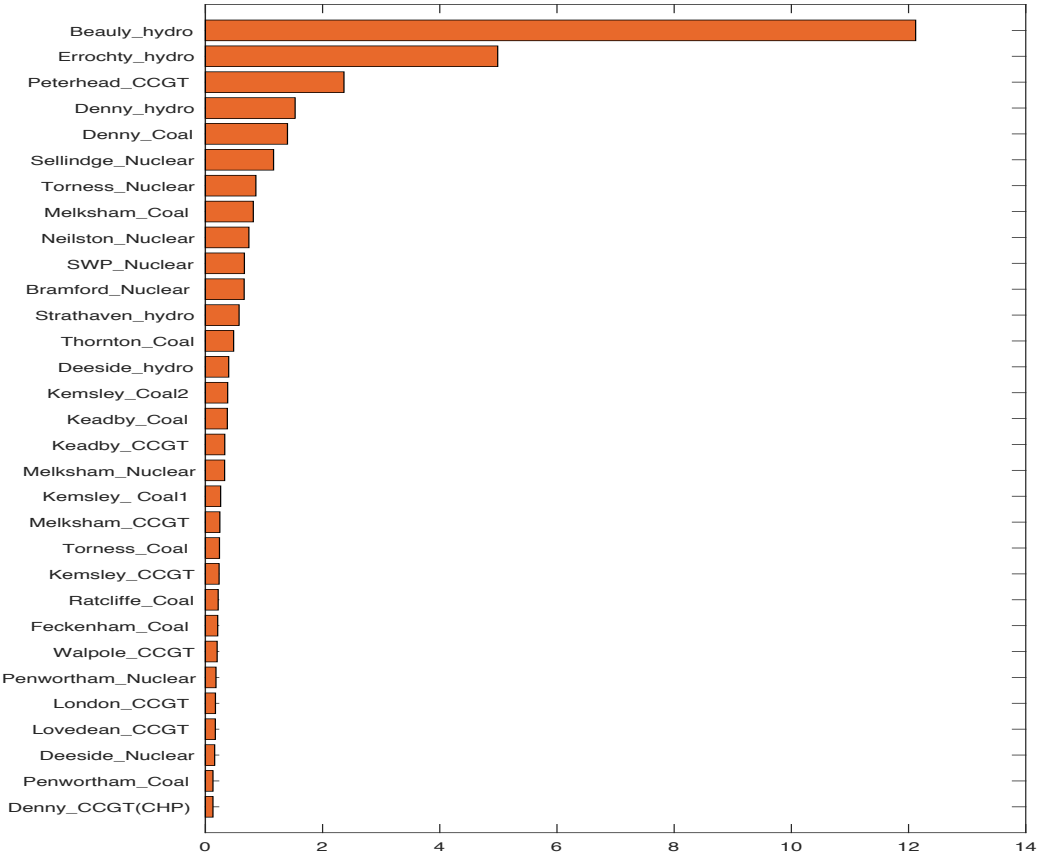

Figure 4.8 Participation factor for mode B

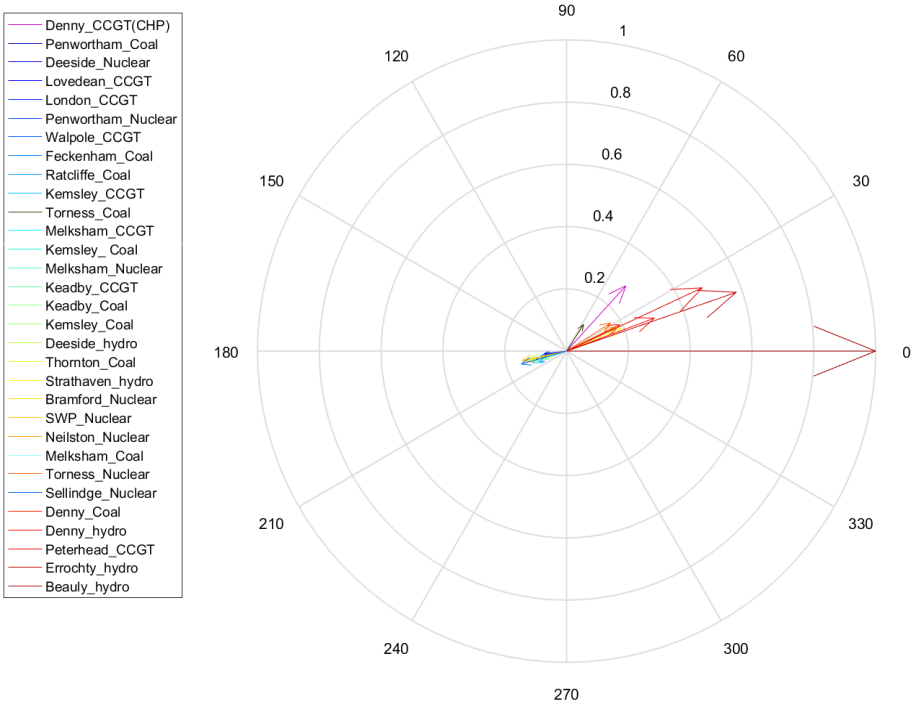

Figure 4.9 Mode shape for mode B

Mode B is an inter-area mode [50], [49] with the generators in the north swinging against those in the south.

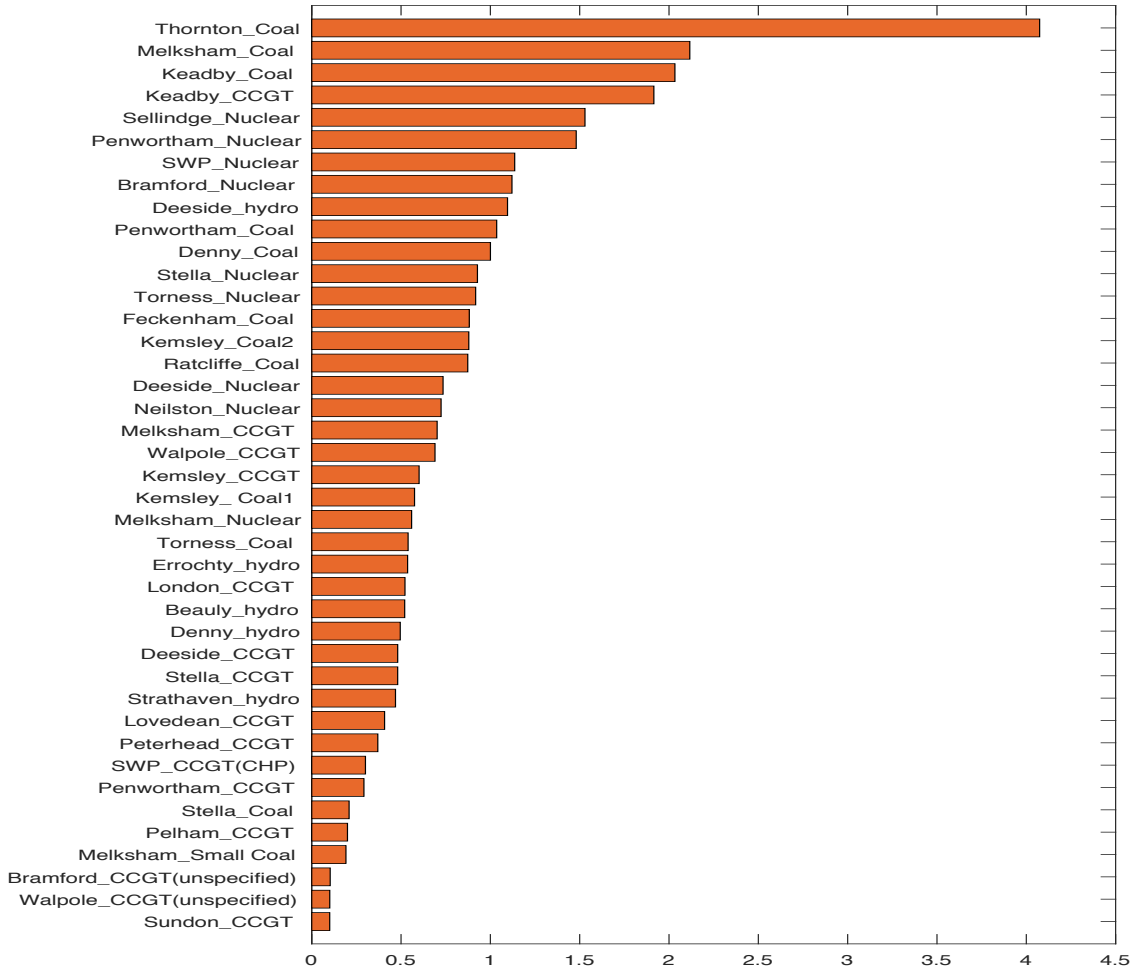

Figure 4.10 Participation factor for mode C

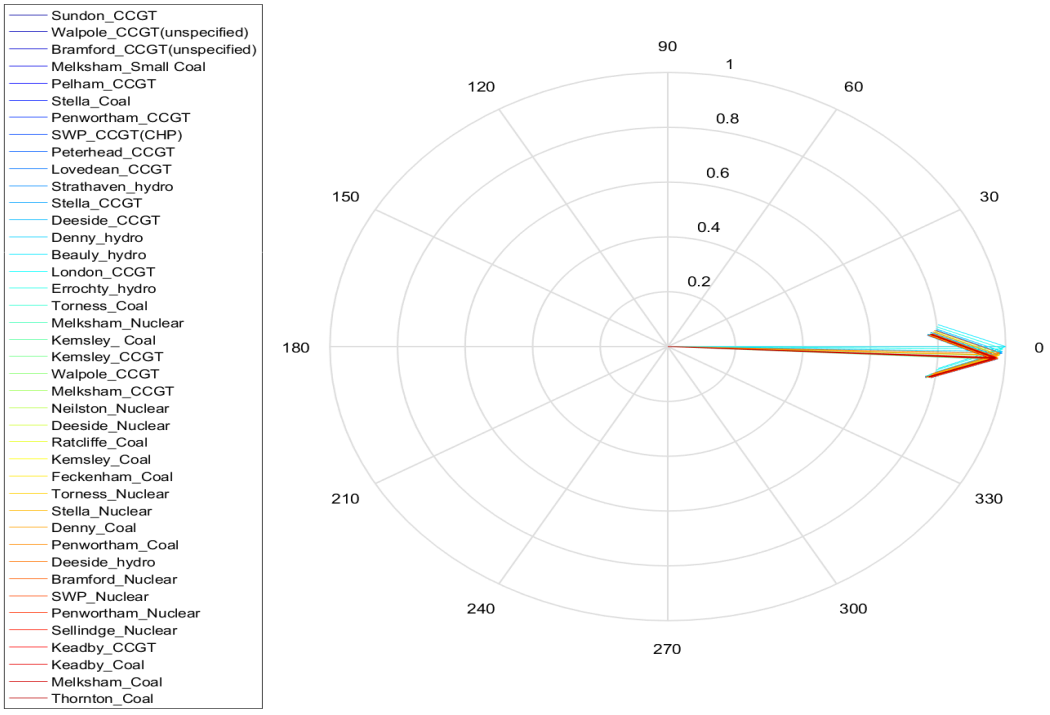

Figure 4.11 Mode shape for mode C

Mode C is a global mode [50], [49] with all the generators moving in unison.

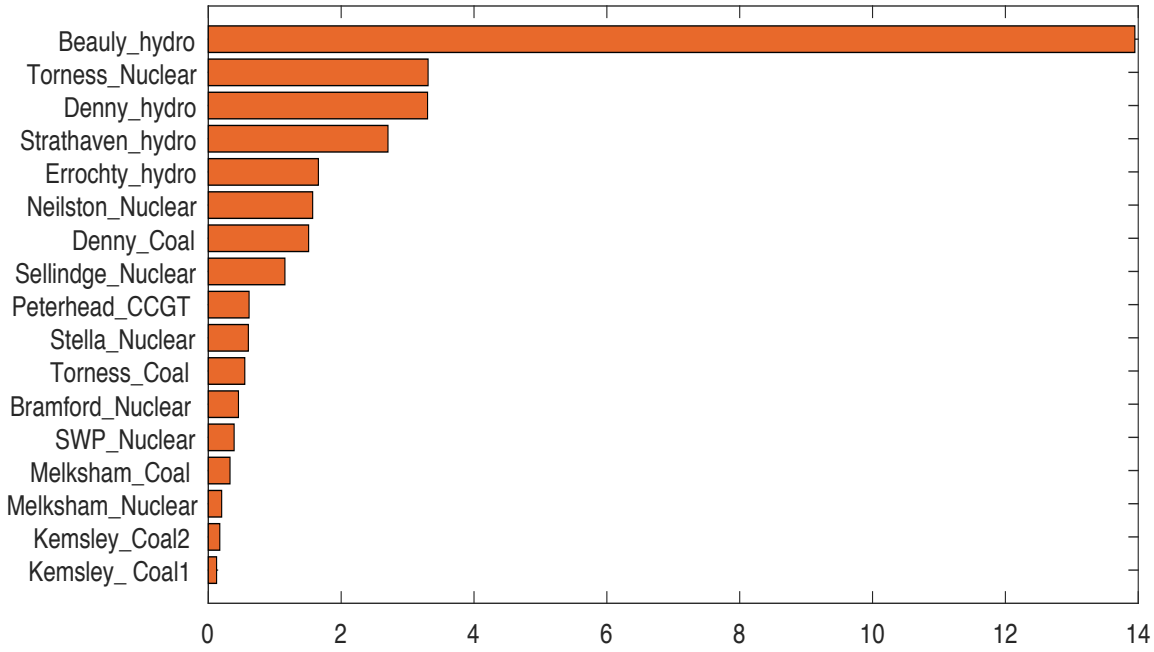

Figure 4.12 Participation factor for mode D

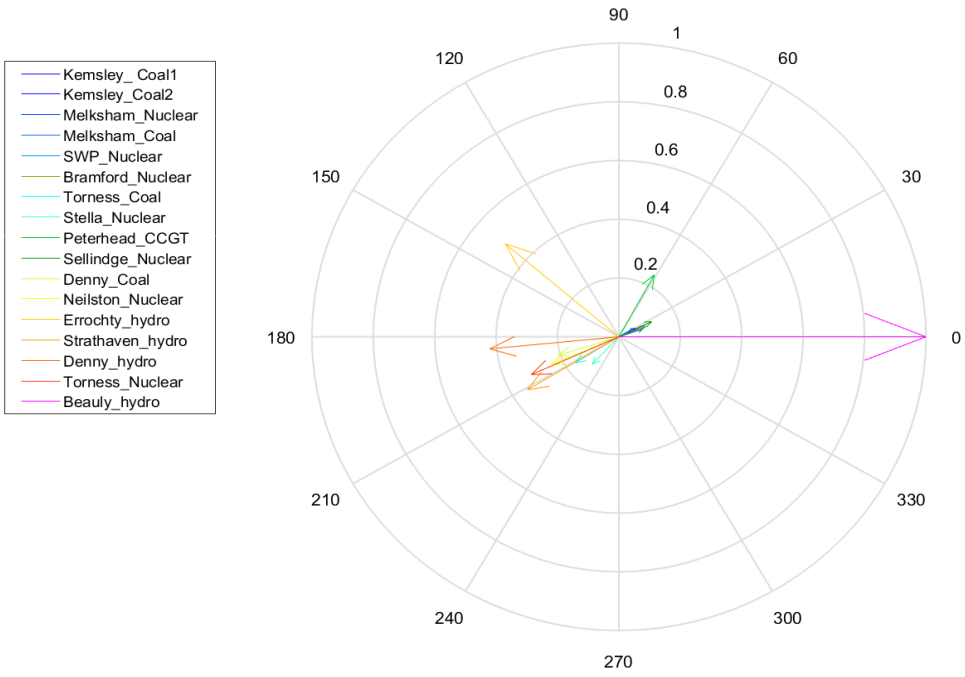

Figure 4.13 Mode shape for mode D

Mode D is another inter-area mode with generators at Beauly, Peterhead, Melksham, Kemsley, Sellindge, SWP, Bramford swinging against the generators at Torness, Stella, Denny, Neilston, Errochty, and Strathaven.

4.3.2 Controller design

4.3.2.1 Input and output signals selection

A wide area controller using robust H_∞ based techniques with pole placement [50], [60] was designed to improve the damping of modes A and B.

In order to design the controller, the generator locations for the controller's input and output signals must be chosen appropriately. It is necessary to select the system's input signals with good controllability for the controller's output and output signals with good observability to serve as stabilising feedback for the controller [50], [60], [49]. The voltage reference of the generators' automatic voltage regulator (AVR) and the rotors' speed deviation were used as the system's input and output signals respectively.

The generators at Beauly, SWP, Errochty, Sellindge, and Keadby are suitable locations since they have relatively high participations in the system's critical modes (from the participation factor plots above). To reduce the number of communication links, the signals with the highest observability and controllability for the modes A and B were chosen after residue analysis [49]. The magnitude of the residues [49] was used as an indication of joint observability and controllability of the modes.

Table 4.2 Magnitude of residues for mode A

		Inputs				
		Beauly	**Errochty**	**Keadby Coal**	**SWP CCGT**	**Sellindge**
Outputs	**Beauly**	2.02×10^{-7}	3.14×10^{-7}	1.91×10^{-5}	7.13×10^{-4}	4.68×10^{-5}
	Errochty	1.40×10^{-7}	2.18×10^{-7}	1.33×10^{-5}	4.95×10^{-4}	3.25×10^{-5}
	Keadby Coal	1.02×10^{-5}	1.59×10^{-5}	9.64×10^{-4}	0.0360	0.0024
	SWP CCGT	0.0011	0.0017	0.1060	3.9554	0.2596
	Sellindge	1.16×10^{-5}	1.80×10^{-5}	0.0011	0.0409	0.0027

Table 4.3 Magnitude of residues for mode B

		Inputs				
		Beauly	**Errochty**	**Keadby Coal**	**SWP CCGT**	**Sellindge**
Outputs	**Beauly**	0.0609	0.0347	0.0084	0.0632	0.0249
	Errochty	0.0354	0.0201	0.0049	0.0367	0.0145
	Keadby Coal	0.0048	0.0027	6.59×10^{-4}	0.0050	0.0020
	SWP CCGT	0.0052	0.0029	7.12×10^{-4}	0.0054	0.0021
	Sellindge	0.0093	0.0053	0.0013	0.0096	0.0038

For mode A, the SWP CGGT generator has the highest controllability and observability, with the generator at Sellindge coming second. For mode B, Beauly and Errochty have the highest observability while SWP and Beauly have the highest controllability.

Consequently, the rotor speed deviations and AVR voltage references of the generators at SWP (CCGT) and Beauly (hydro) were chosen as the appropriate signals.

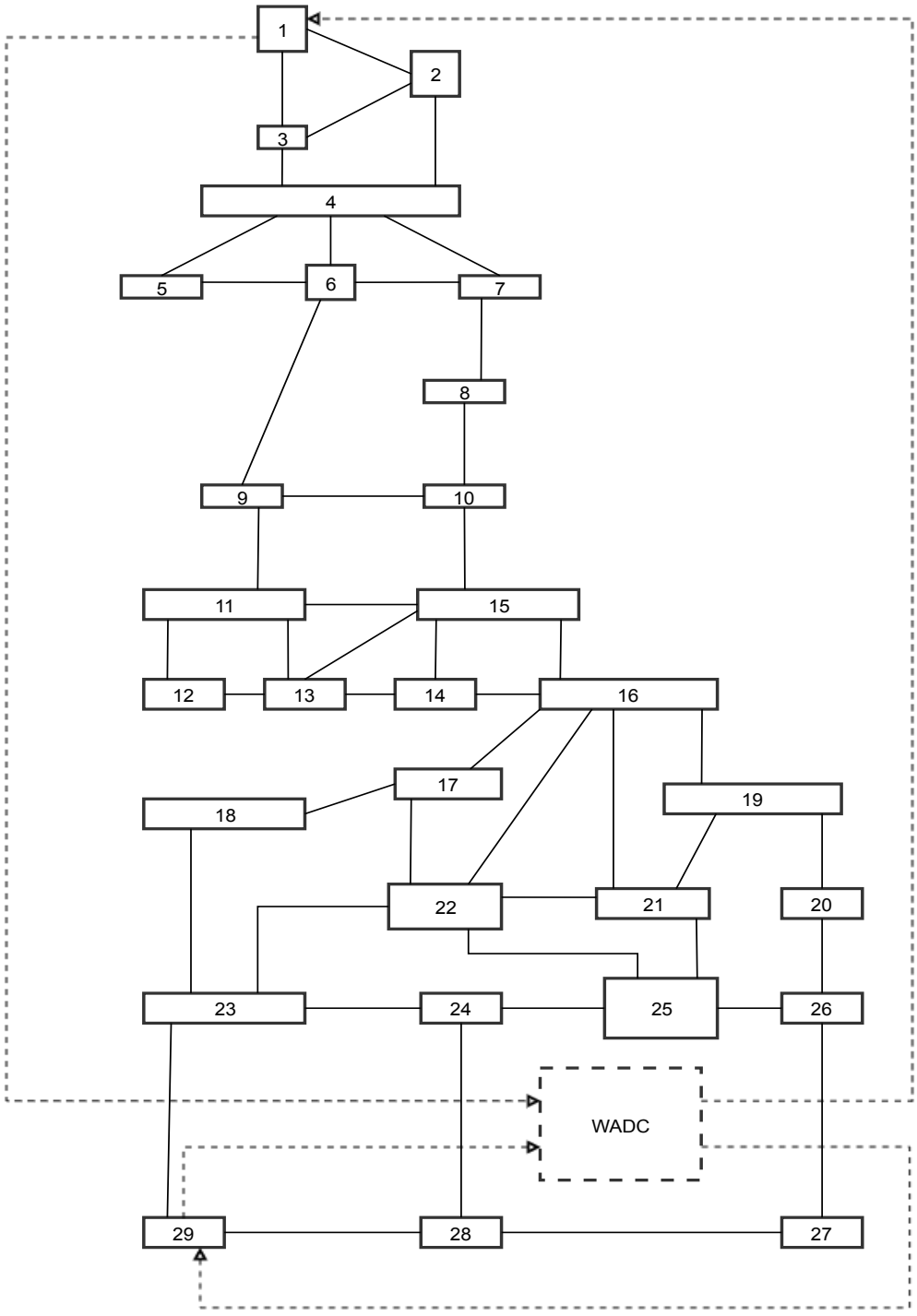

Figure 4.14 Representative GB network with wide area damping controller

4.3.2.2 Weight selection and synthesis

In conformance with standard H_∞ mixed-sensitivity design practices [50], a low pass filter was selected to improve output disturbance rejection while a high pass filter was used to reduce the control effort outside the frequency range of interest, as highlighted previously in Section 3.3.2.

The transfer functions for the weights and corresponding bode diagram plot are given below.

$$W_1(\mathrm{s}) = \frac{10}{s+10}\,, \qquad W_2(\mathrm{s}) = \frac{s}{s+100}$$

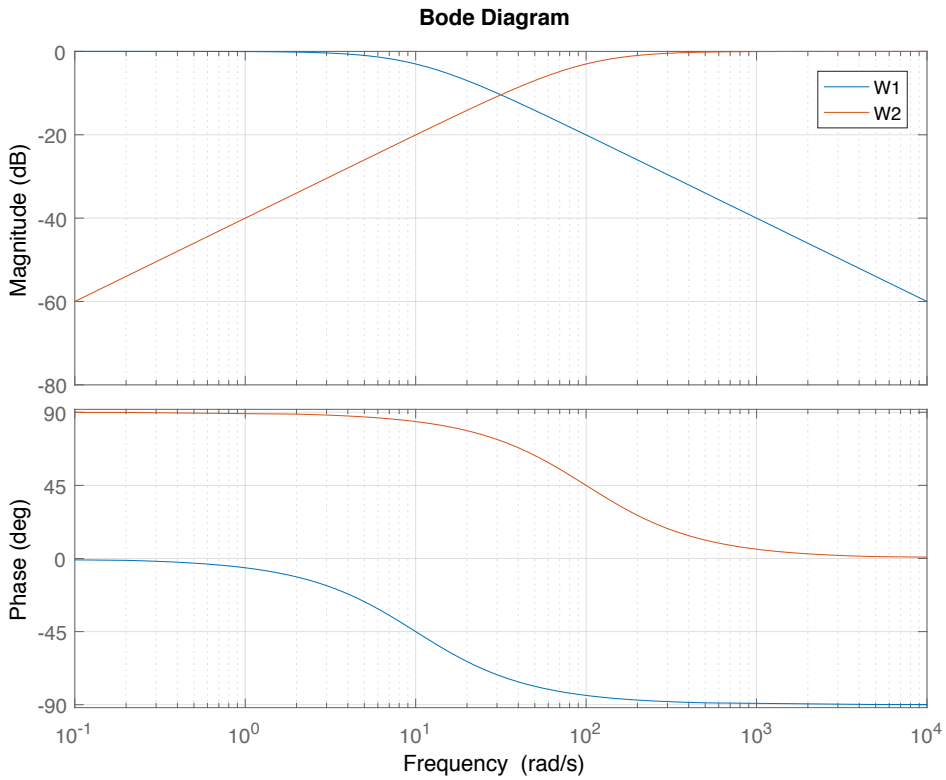

Figure 4.15 Bode diagram of weighting functions

Before synthesising the controller, the initial 797 state model was reduced to an equivalent model containing only 18 states using balanced model reduction[1] tools from MATLAB's robust control toolbox [75]. This is necessary in order to reduce computation time and control effort [50], [60]. Figure 4.16 shows the frequency response of the original and reduced models.

[1] The energy of the states of a system is denoted by Hankel Singular Values (HSV) (from control theory [50]). By examining the HSV, the least significant states, which have negligible effect on the system input/output behaviour, can be discarded, resulting in a system with lower order. For a good approximation, the difference between the H_∞ norm of the reduced and original model must be small [50]. [50], [85], [86] describe balanced model reduction more extensively.

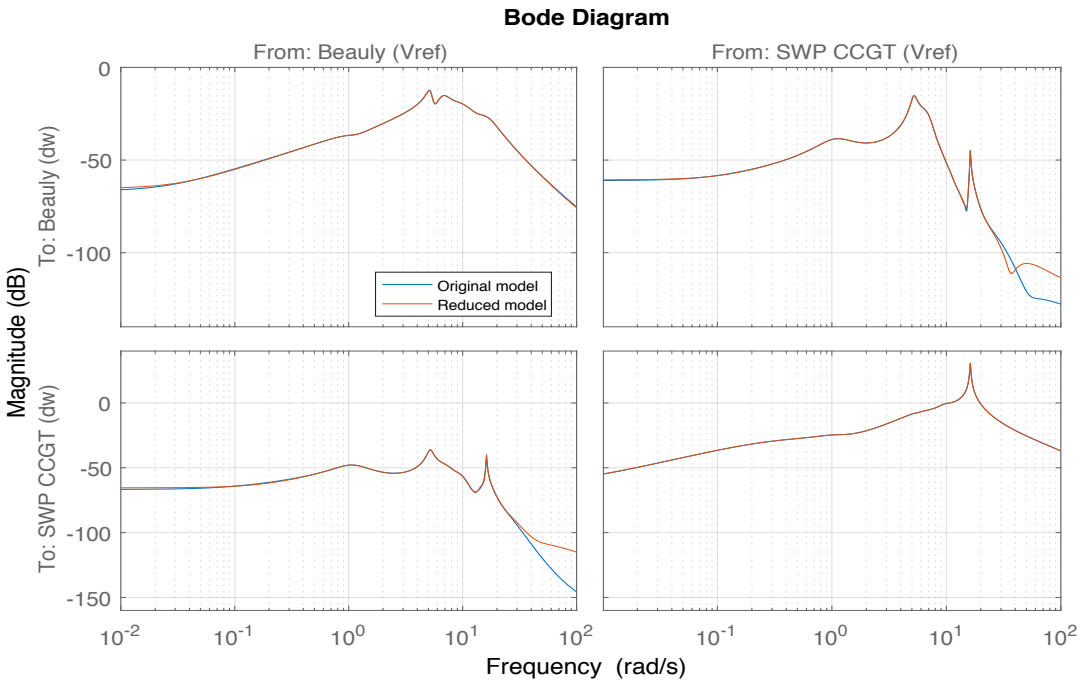

Figure 4.16 Frequency response of original and reduced model

As evidenced from Figure 4.16, the reduced model adequately approximates the full order model within the frequency range of interest.

With the weights selected and the full order model reduced, the controller is then synthesised using H_∞ synthesis tools from MATLAB's robust control toolbox [76], [77]. The controller places the modes that are observable and controllable from the system's output and input signals on the region of the complex plane that ensures a minimum damping ratio of 10%. This region on the complex plane is defined by a conic sector lying in the left-hand plane with its tip at the origin and having an inner angle of $2\times \cos^{-1} 0.1\ rads$ [50]. The program code for the controller synthesis is given in Appendix B.3.

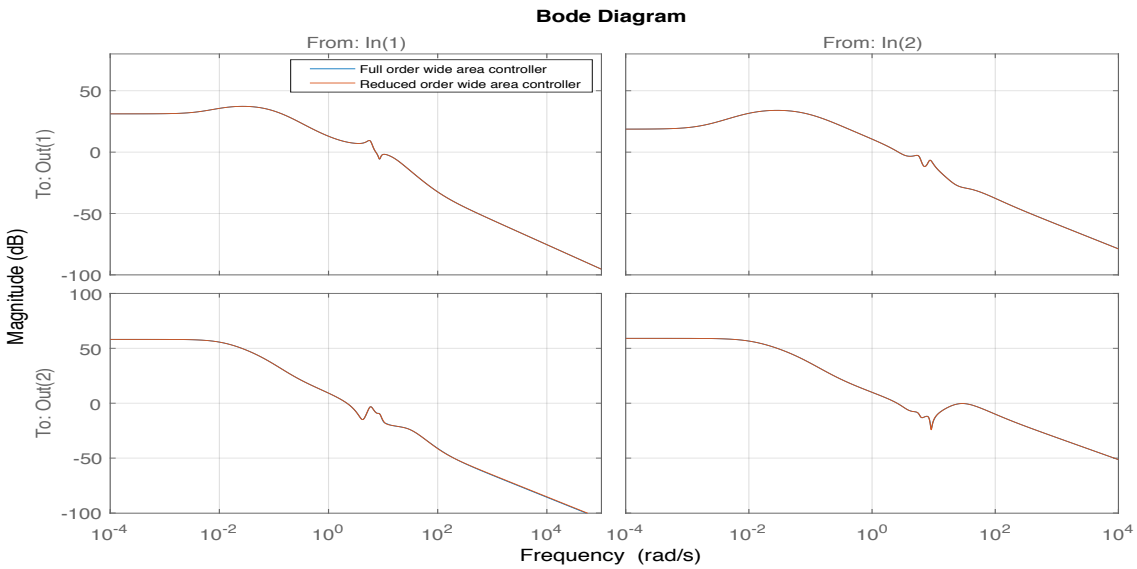

Figure 4.17 Frequency response of full and simplified controller

The resulting controller contains 22 states, which is equal to the order of weights plus that of the reduced model.

The controller was then simplified to 16 states, using the procedures described above, without sacrificing performance, as evidenced in the frequency response shown in Figure 4.17. Also, an appropriate washout filter was used to minimise the controller's actions during slow changes in system frequency in steady state [49].

4.3.2.3 Eigenvalue plot

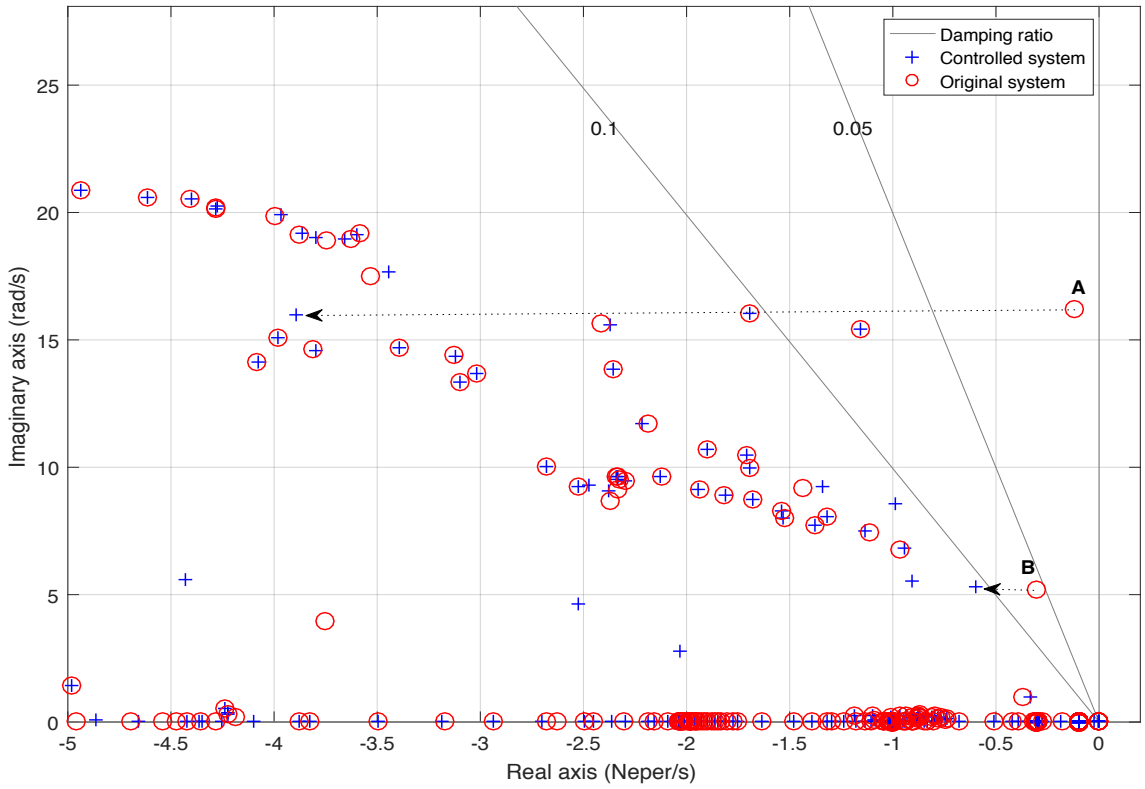

Figure 4.18 Plot of eigenvalues of system with designed controller

The designed controller is added to the model and the combined system is again linearized. From the resulting eigenvalue plot in Figure 4.18, it can be seen that the damping of the system has been improved.

The previously lightly damped mode A has been moved far into the left half plane, shortening the modes decay time. Also, the damping ratio of the inter-area mode B has been increased to more than 10 %.

Modes B and C, however, are relatively unchanged. This is as a result of the choice of the controller's input and output signals, which had limited observability and controllability of the modes. However, this is acceptable as the modes were already heavily damped.

The improvement in the system's small signal response is verified with a time domain simulation of the full nonlinear system in the next section.

4.3.3 Time domain simulation

4.3.3.1 Without wide area controller

At 0.1 seconds, a three-phase short circuit fault was applied at the SWP node, and it is cleared after 15 milliseconds. This was done to excite the modes [49] to allow for verification of the controller's performance.

The time domain response of the speed deviation of the Beauly, Errochty, SWP CCGT, Keadby Coal, and Sellindge generators are shown in Figure 4.19.

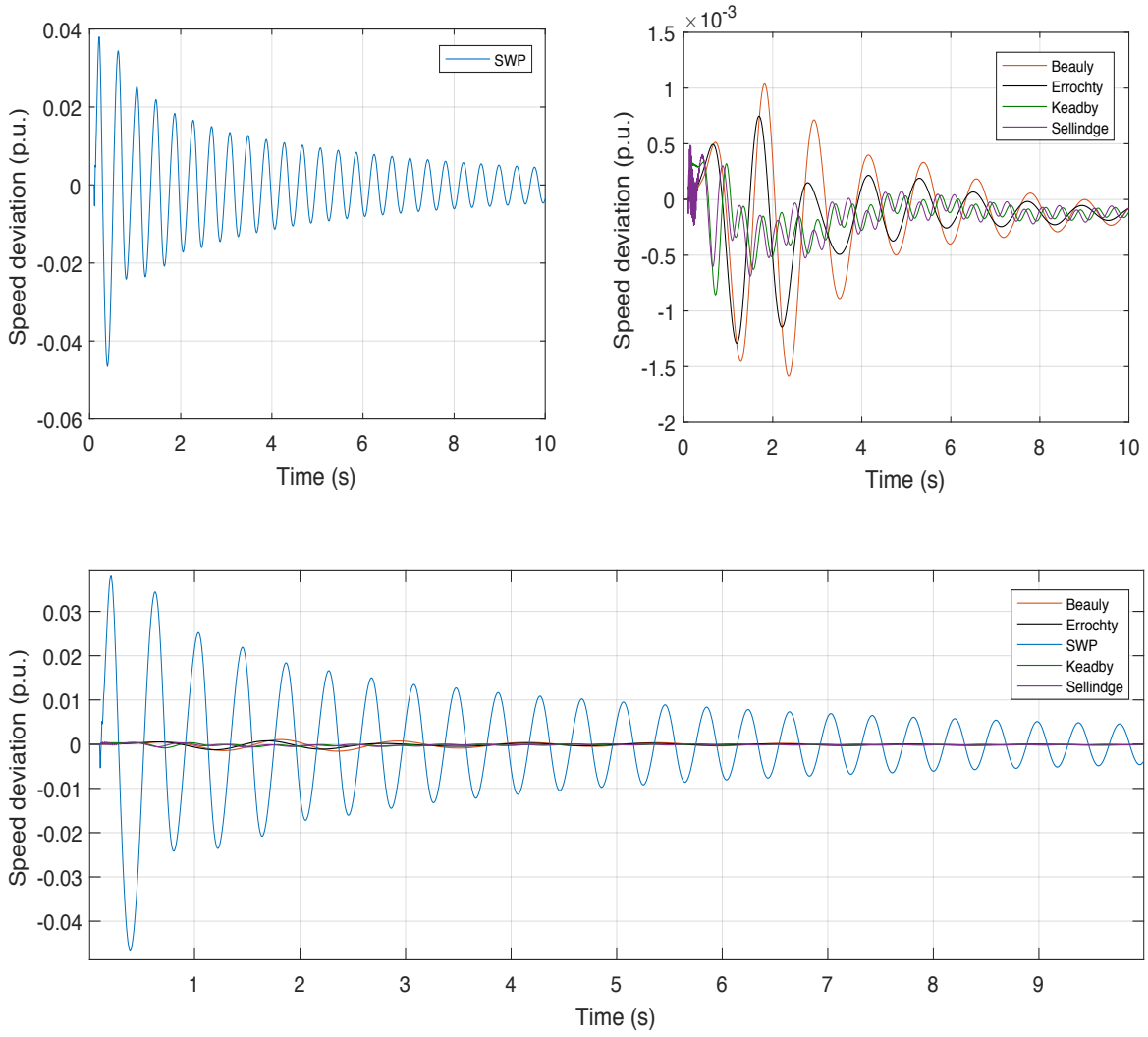

Figure 4.19 Generators' speed deviation time response

As evidenced from Figure 4.19, the system's damping is poor before the introduction of the wide area controller, with the oscillation not completely decaying even after the fault has been cleared for more than 10 seconds.

The generators' terminal voltage responses are shown in Figure 4.20 below.

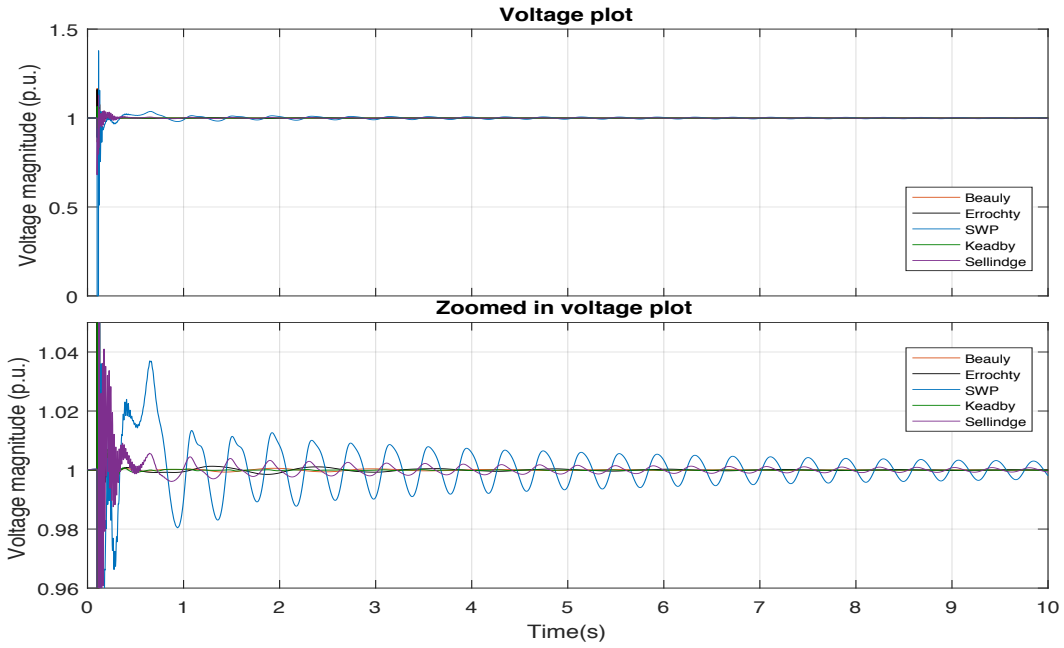

Figure 4.20 Generators' terminal voltage time response

4.3.3.2 With wide area controller

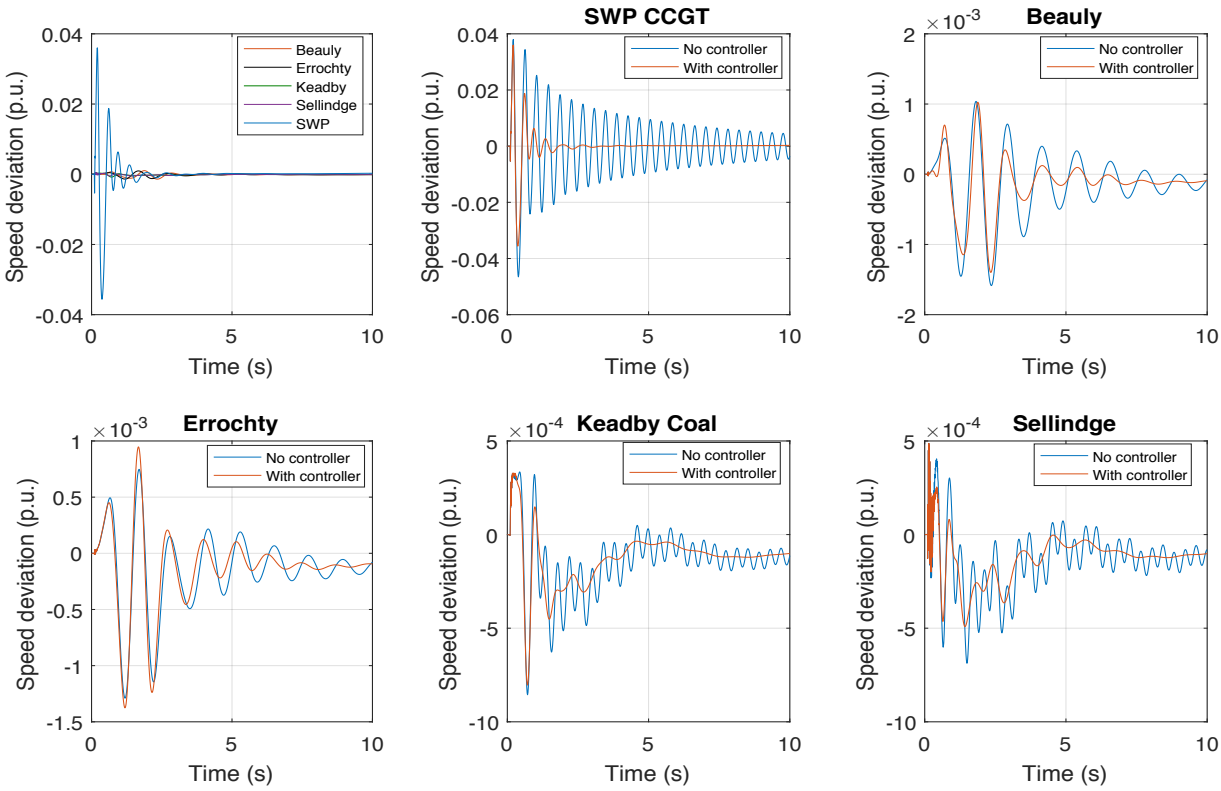

Figure 4.21 Generators' speed deviation time response with wide area controller implemented

With the introduction of the wide area controller, the system's damping is improved; this is especially true for the generators close to the SWP node.

The generators' terminal voltage responses with the wide area controller implemented are shown in Figure 4.22.

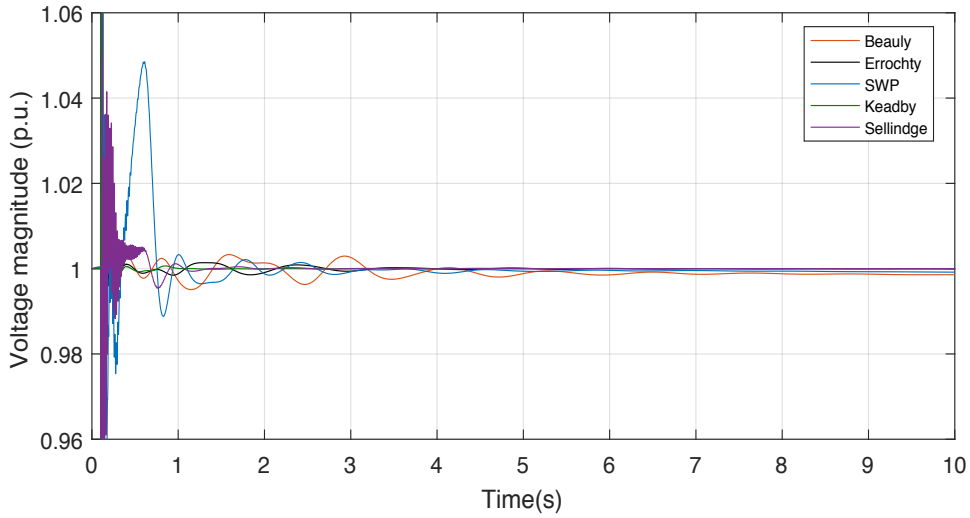

Figure 4.22 Generators' terminal voltage time response with wide area controller

4.3.4 Effects of time delay

4.3.4.1 Constant time delays

For the initial evaluation of the effects of time delay on the system's small signal performance, constant time delays were added to the controller's communication links in its input and output paths. This is illustrated in the figure below. Here, Ts represents the one-way time delay while the total delay 2·Ts.

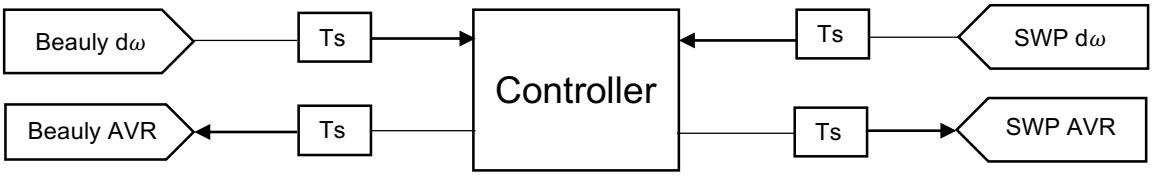

Figure 4.23 Illustration of the wide area controller with time delays in its input and output paths

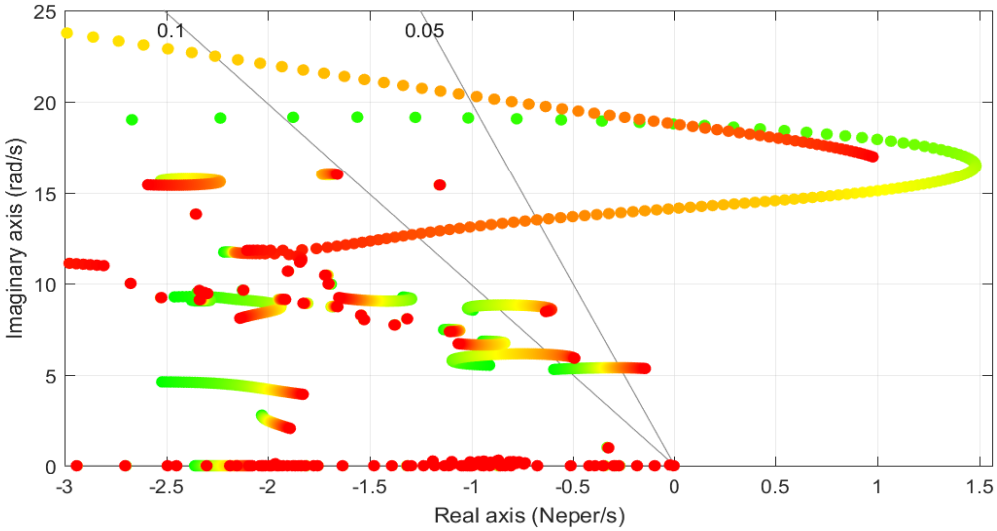

Figure 4.24 Eigenvalues plot with increasing constant time delays

These time delays were incrementally increased from 1 to 250 milliseconds, resulting in a total of 2 to 500 milliseconds delay for each complete signal path. At each value of the time delay, the system was linearized at the initial operating point and its eigenvalues were plotted. This plot is shown in Figure 4.24, with the green-through-red colour spectrum representing the increase in Ts from 1 to 250 milliseconds.

The introduction of the time delays results in new modes at higher frequencies. Generally, the increase in time delays results in the increase of the real parts of the eigenvalues in the positive direction (i.e. towards the unstable right-hand region), worsening the modes' damping ratio and increasing their decay time. For higher values of the time delays, the system reaches unstable operation as some eigenvalues eventually reach the right-hand plane.

4.3.4.2 Actual communication time delays

With the addition of the actual communication time delays, the system becomes small signal unstable. This is observed in the eigenvalues plot shown below, where the real part of a complex conjugate pair of eigenvalues lies on the right-hand of the complex plane.

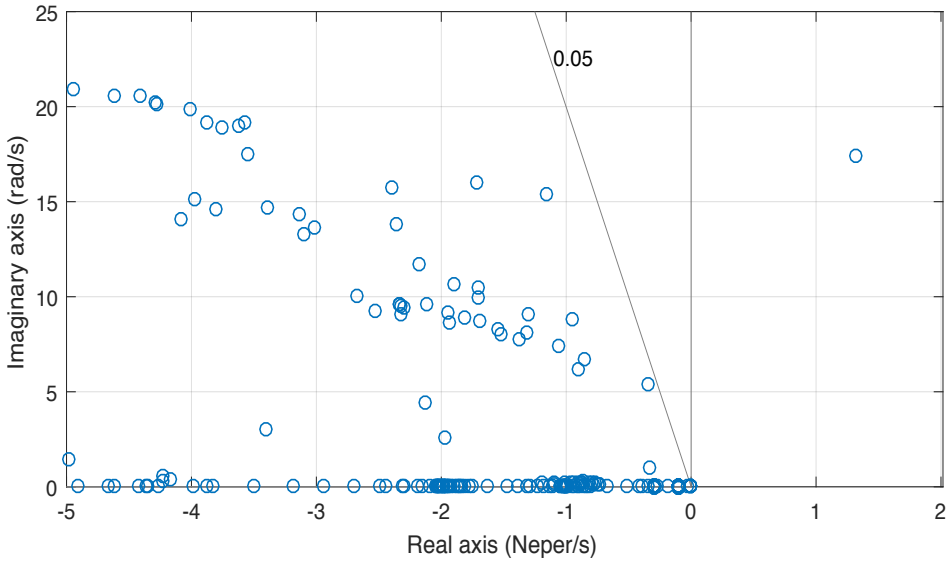

Figure 4.25 Plot of eigenvalues with actual communication time delays

Table 4.4 Actual communication time delays for wide area controller signal paths

Sending node	Receiving node	Time delay (milliseconds)
Beauly	London	123.1
SWP	London	60.9

This instability is observed in the step response of the linearized model shown in Figure 4.26.

The linear system is seen to be unstable to a step in the voltage reference of the SWP CGGT generator AVR, with the oscillations of the generators' speed deviations growing without bounds.

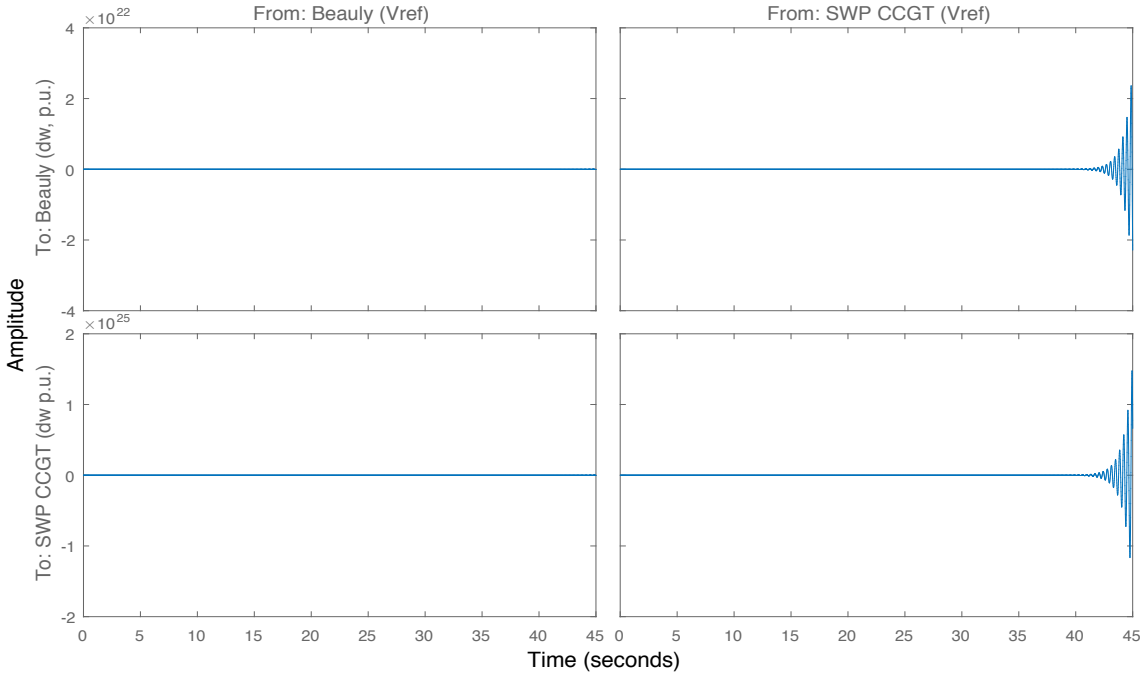

Figure 4.26 Step response of linearized system with actual communication time delays

The time domain simulation of the full nonlinear system also shows the instability. With a 15 milliseconds fault applied at the SWP node, the speed deviations of generators exhibit growing oscillations leading to instability. This is shown in Figure 4.27.

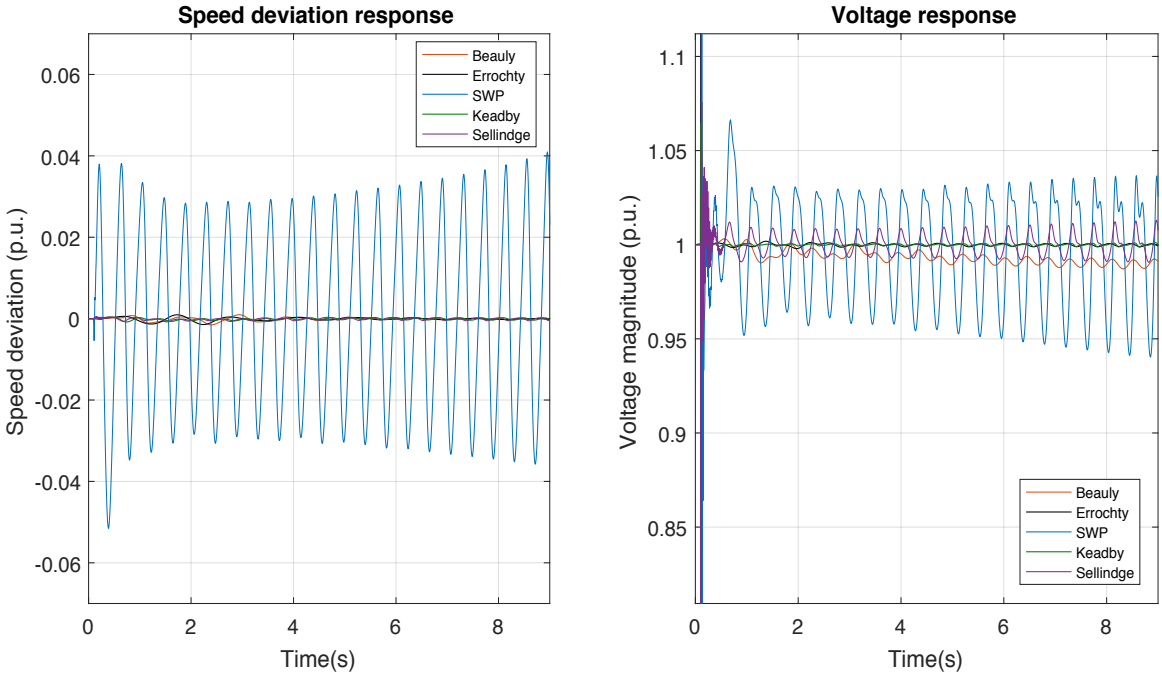

Figure 4.27 Generators unstable time response with communication time delays

4.3.4.3 Other cases

4.3.4.3.1 Modified wide area damping controller (WADC) for inter area mode B with reference loading

To minimise the effect of the time delays, the wide area controller was redesigned to focus its control effort on the inter-area mode, which is a more popular application in the literature [50], [60], [64].

To this end, a local area power system stabilizer (PSS) was designed using the residues method [49] to improve the damping of mode A. The PSS input and output signals were selected in a similar fashion to the wide area design described previously. The deviation of the SWP CCGT generator's rotor speed from the synchronous speed was chosen as the PSS stabilising signal and its output was connected to the generator's AVR.

PSS design

The residue from the speed deviation of the SWP CCGT generator to the AVR voltage reference is

$$Rc_A = 1.5839 - j3.6246$$

with an angle of $-66.40°$.

To move the mode to the left (thereby increasing its damping), an additional phase lag of 113.6º is required. In addition, a washout filter with a time constant of 6 seconds is included to ensure the generator's terminal voltage does not stray from its reference value due to slow changes in system frequency in the steady state [49]. This washout filter introduces a phase lead of 0.59º. Therefore, the PSS must introduce a total phase lag compensation of 114.19º at the complex frequency of mode A ($\lambda_A = -0.1165 + j16.1938$).

This phase compensation was implemented with two phase lag compensators (with each introducing a phase lag of 57.095º). The designed lag compensators have the following form [49]

$$K(s) = \frac{T_1 \cdot s + 1}{T_2 \cdot s + 1}\Bigg|_{s=-0.1165+j16.1938}$$

The designed compensators had $T_1 = 0.0182\ s$ and $T_2 = 0.2042\ s$. A gain of 4 was selected as it ensured a minimum damping of 5 % for mode A without significantly deteriorating the damping of the other modes. The resulting system eigenvalues plot with the addition of the local PSS is shown in Figure 4.28 below.

With the PSS added, the damping of mode A improves to 6.4 % but that of mode B decreases slightly, though it remains slightly higher than 5 %.

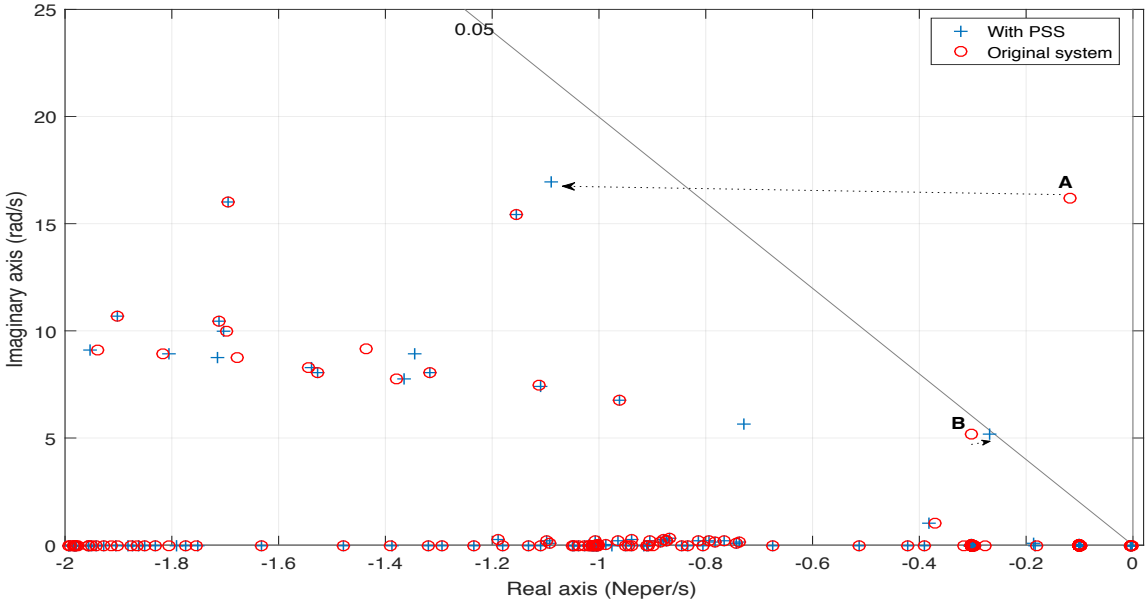

Figure 4.28 Plot of system eigenvalues with local PSS

WADC synthesis

The system with the PSS added was then linearized and the WADC was synthesised focusing on the control of the inter area mode B by modifying the previous weighting functions used. The modified weights are given below:

$$W_1(s) = \frac{36}{s^2 + 8.4s + 36}, \qquad W_2(s) = \frac{10s}{s + 10}$$

The cut-off frequency of the low pass filter was reduced to 6 rad/s in order to focus on frequencies below that value, while that of the high pass filter was also reduced to a lower value, resulting in a minimisation of the control effort at a lower frequency than in the previous design. The frequency response of the modified weights is shown below.

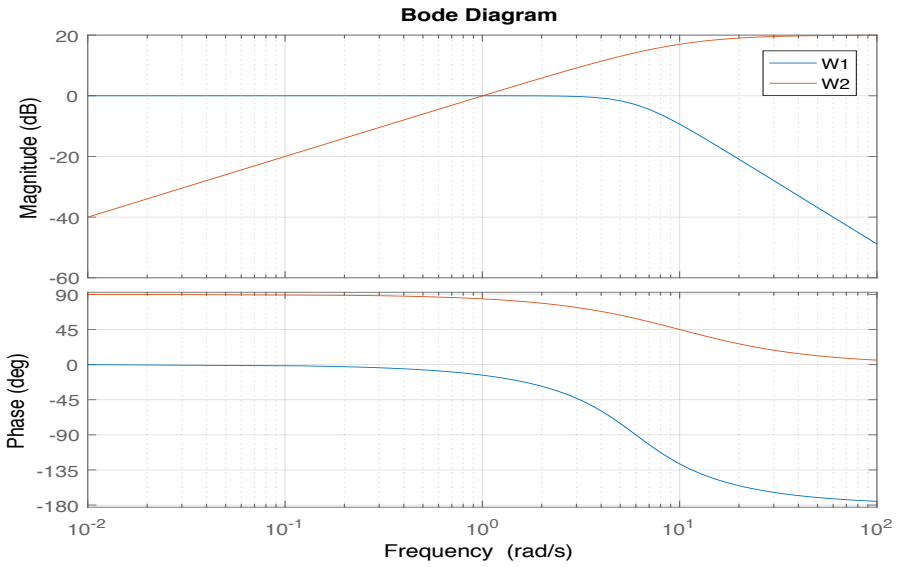

Figure 4.29 Frequency response of modified weighting functions

Aside the modified weights, the WADC design procedure is the same as previously described. The eigenvalues plot in Figure 4.30 shows the improvement in the damping of the inter area mode B with the addition of the WADC.

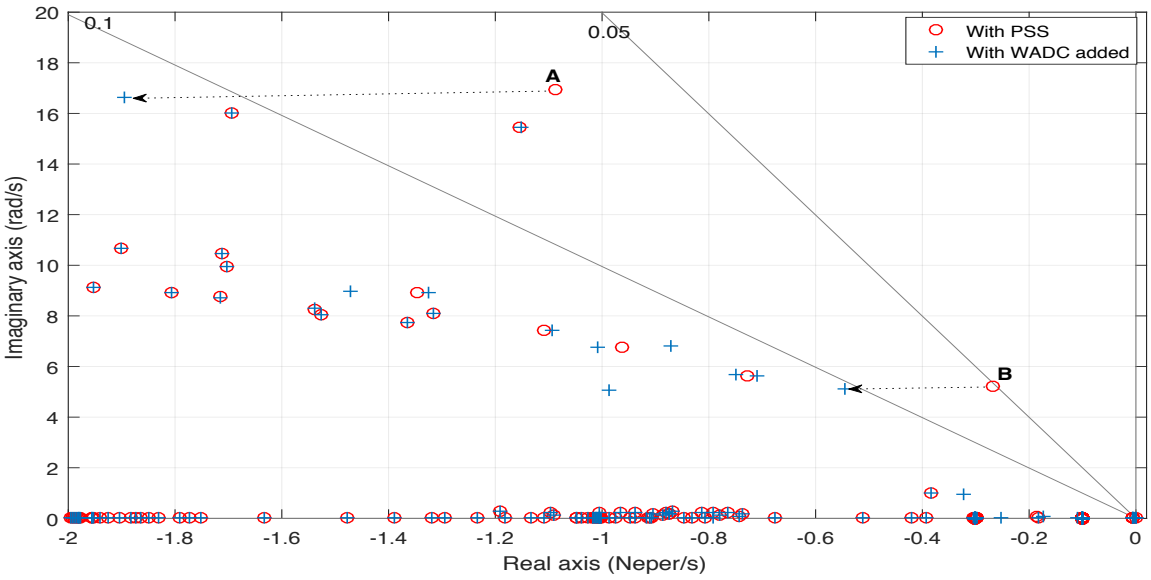

Figure 4.30 Plot of system eigenvalues with WADC

Similar to the previous case, constant time delays were introduced to the WADC in order to observe its effects during operations. With the modified weights focusing on the control of the inter area mode, the time delays no longer lead the system to unstable operation. However, increasing time delays still degrades the WADC performance, resulting in reduced damping of the modes and slower oscillation decay time. This is clearly evident in Figure 4.31.

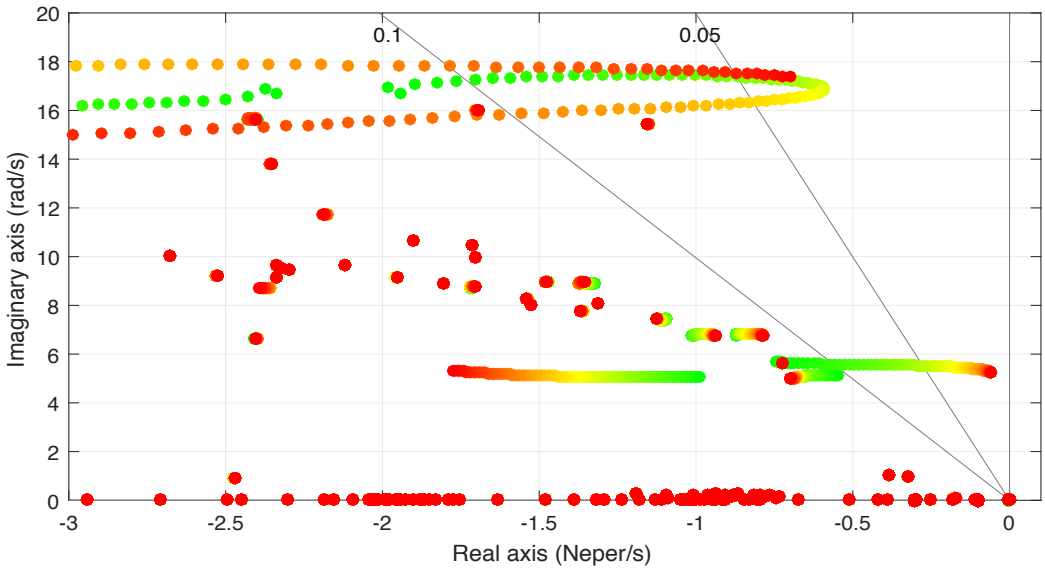

Figure 4.31 Eigenvalues plot with increasing constant time delays for modified WADC

Actual communication delays

The actual communication delays were added to the WADC with the modified weights. The resulting eigenvalues plot for the system is shown below.

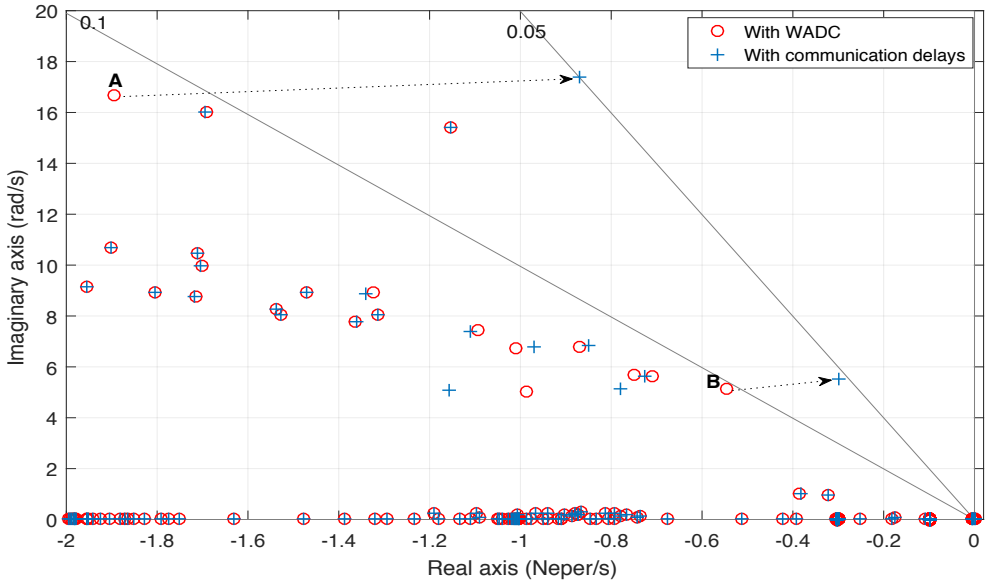

Figure 4.32 Plot of eigenvalues with actual communication time delays for modified WADC

In this case, although there is some degradation in performance, the system is small-signal stable with damping of about 5 % for modes A and B.

Figure 4.33 shows the time domain response of the active power flowing from Scotland to the South (through the transmission lines connecting Nodes 8 to 10 and Nodes 6 to 9). This shows the active power oscillations with and without the actual communication delays.

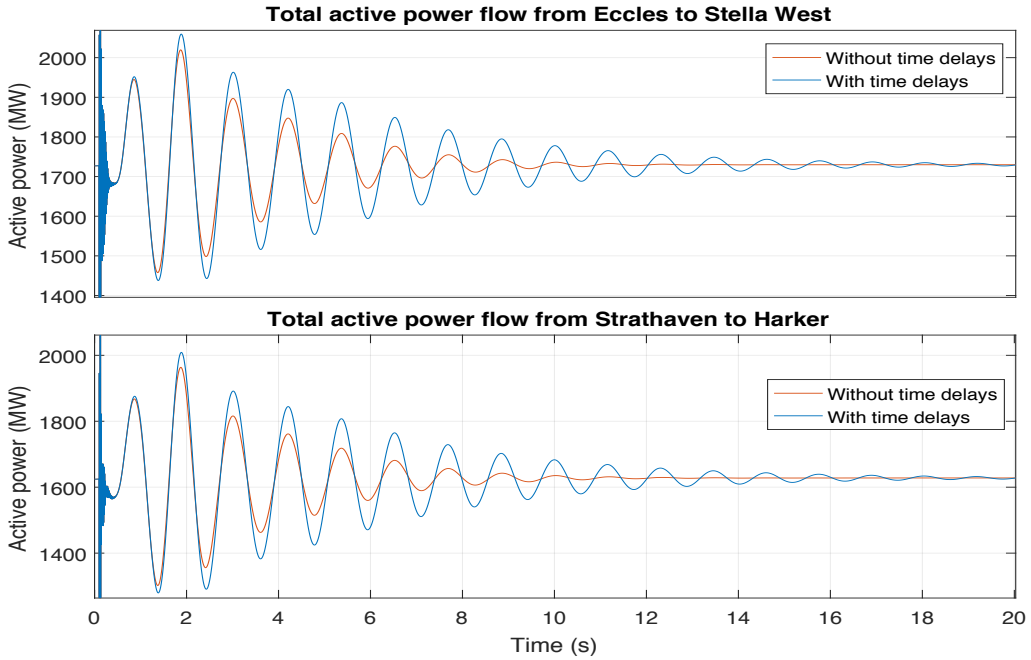

Figure 4.33 System time response of modified WADC with and without communication delays

4.3.4.3.2 Stressed system

The system is stressed by increasing the power transferred from Scotland to the South. This is done by decreasing the active power loading of the nodes in Scotland (Nodes 1 – 8) in equal steps of 10 percent and increasing the load in the remaining 21 nodes (Nodes 9 – 29) by an equal amount [36].

For each load change step, the effect of the actual communication delays on the WADC was investigated. Two scenarios for the communication delays were considered. The first case was for low network traffic on the UK fibre communication system (which has been utilised for the previous cases examined thus far), and the second was for high network traffic on the communication network. The results of these scenarios are summarised in Table 4.6 and the active power flows under the different network traffic scenarios are shown in Figures 4.34 and 4.35.

However, as noted previously, the change in time delay due to background traffic is very small. The time delays for the high demand case is shown in the table below.

Table 4.5 Communication time delays for high network traffic scenario

Sending node	Receiving node	Time delay (milliseconds)
Beauly	London	137.3
SWP	London	61.5

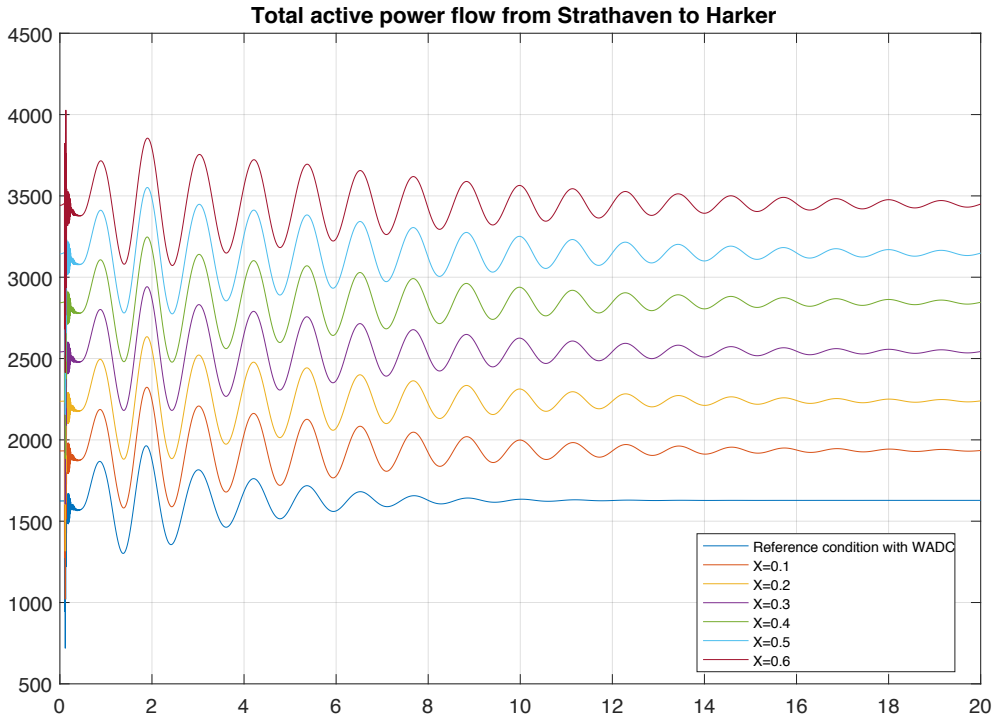

Figure 4.34 Active power flow with increasing stress for low network traffic scenario

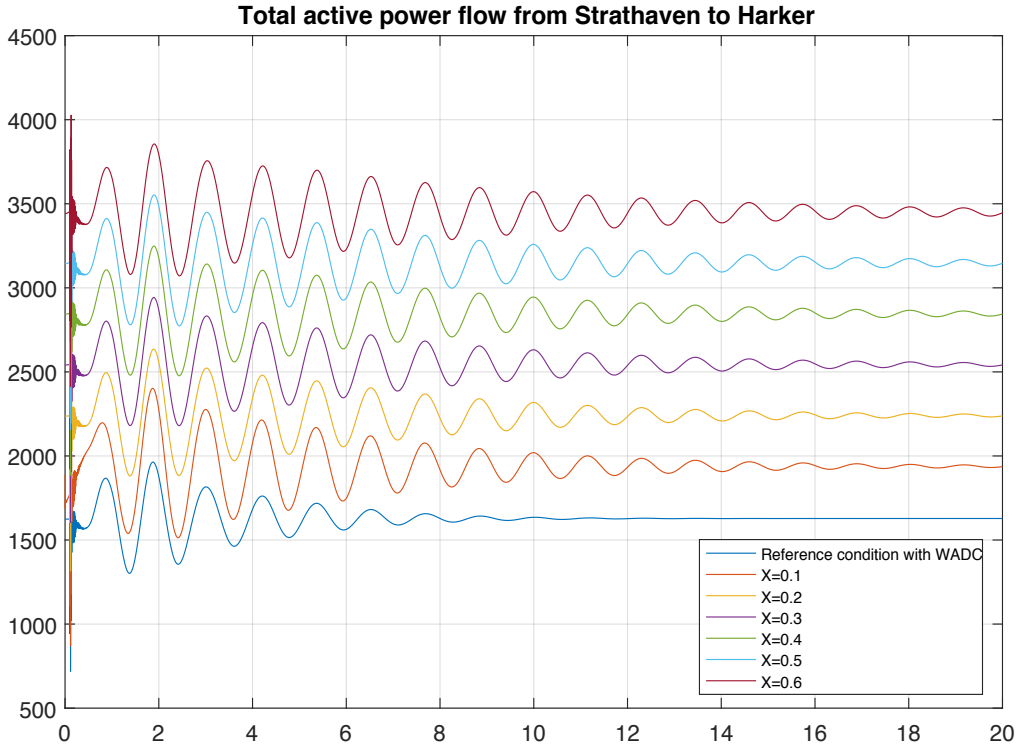

Figure 4.35 Active power flow with increasing stress for high network traffic scenario

Table 4.6 Effects of communication delays on mode B with increasing system stress

Scenario		WADC without time delays			WADC with actual communication delays		
		Eigenvalue	Frequency (Hz)	Damping (%)	Eigenvalue	Frequency (Hz)	Damping (%)
x=0.1	Low network traffic	-0.5582 ± j5.137	0.82	10.80	-0.2771 ± j5.498	0.88	5.03
	High network traffic				-0.2615 ± j5.486	0.87	4.76
x=0.2	Low network traffic	-0.5682 ± j5.158	0.82	10.95	-0.2606 ± j5.500	0.88	4.73
	High network traffic				-0.2452 ± j5.489	0.87	4.46
x=0.3	Low network traffic	-0.5745 ± j5.179	0.82	11.03	-0.2445 ± j5.499	0.88	4.44
	High network traffic				-0.2294 ± j5.488	0.87	4.18
x=0.4	Low network traffic	-0.5784 ± j5.202	0.83	11.05	-0.2294 ± j5.498	0.88	4.17
	High network traffic				-0.2145 ± j5.487	0.87	3.91
x=0.5	Low network traffic	-0.5779 ± j5.227	0.83	10.99	-0.2151 ± j5.495	0.87	3.91
	High network traffic				-0.2005 ± j5.485	0.87	3.65
x=0.6	Low network traffic	-0.5696 ± j5.252	0.84	10.78	-0.2019 ± j5.491	0.87	3.67
	High network traffic				-0.1873 ± j5.481	0.87	3.42

It can be observed that the designed wide area damping controller is very robust for the different operating conditions. The WADC provided a relatively constant damping of 10.8 % for all the operating conditions considered. However, its performance is degraded when the communication time delays are introduced, with the damping going as low as 3.42 % for the heavily stressed loading case during high network traffic. The oscillations also decay slower when the time delays are introduced. For the most stressed condition examined (x=0.6, and high network traffic), the time taken for the amplitude of the oscillations to decay by half increases by approximately 300 % from 1.22 seconds without time delays to 3.70 seconds with time delays (for the high demand case).

Nevertheless, the system remains small-signal stable for all the operating scenarios considered.

Chapter 5
Conclusions and future work

5.1 Conclusions

In this work, a reduced model of the Great Britain transmission network and the UK (BT) core communication network has been co-simulated using the MATLAB/Simulink software. A steady-state representative GB transmission network (RGBN) from [10] was initially modelled and validated. To facilitate stability studies, generator dynamics, parameterised with data from [54], were added to the steady-state RGBN model. Generator controls (excitation systems and governor turbine models) and transformers connecting the generators to the network were similarly added.

To ascertain the effect of the communication network on the small-signal stability of the RGBN model, a centralised wide-area controller was designed to dampen generators' rotor oscillations. Time delays in the wide-area controllers' communication links were accounted for by using a MATLAB heuristic function that calculates the delay between the UK (BT) Core network nodes [58], [12]. The wide-area damping controller (WADC) design was defined as a robust H_∞ mixed-sensitivity with pole placement problem which was solved numerically by the linear matrix inequality approach. Detailed design procedures for the WADC were presented.

The time delay effects were investigated on the RGBN model with only the WADC installed and with the WADC complemented by a power system stabilizer acting locally. Nonlinear time-domain simulations and eigenvalue analysis were both used in the stability assessment.

Several conclusions can be made from the obtained results. First, the magnitude of the residues for a specified mode can be effective in selecting the feedback stabilising signals for the WADC and in determining the locations for the controller's output signals.

Furthermore, a wide-area damping controller designed by the H_∞ mixed-sensitivity control with pole placement can have better damping performance than a system controlled with only locally installed power system stabilizers (PSSs). Also, the WADC designed by H_∞ control shows robust damping performance to changes in system operating conditions. However, the WADC is sensitive to communication time delays and may lead the power system to unstable operation for sufficiently high time delays.

The damping of the system can become more resilient to the effects of communication time delays by installing local PSSs in conjunction with the WADC. Nevertheless, communication

time delays result in substantial deterioration of the system's rotor oscillations damping when controlled with WADC with or without local PSSs in operation.

Hence, communication time delays affect the small-signal stability of the power system. Consequently, it can be necessary to study the cyber-physical system interactions via simulations as the communication network may result in undesirable operation of the physical power system.

5.2 Future work

Although the results obtained produced valuable information to assess the effects of the communication time delays on the small-signal stability of a power system, further research on the work can be made.

State estimation

In practice, full power system models are not typically available when designing wide are damping controllers. Perfect information about the states of the system may not be obtainable and would need to be estimated [78], [79]. Hence, it may be necessary to design the WADC for this practical scenario [80]–[82] and beneficial to investigate the effects of the communication delays for this case.

Robustness to time-delays

With the WADC designed with imperfect system state information, the effects of communication time delays may become more pronounced. As a result, it may become essential to design the wide area damping controller to be robust to the time delays. Reference [60] describes a robust WADC designed with time delay modelled as an uncertainty while [50] describes the use of the unified Smith predictor for designing an H_∞ based WADC that is robust to time delays. The performance of such a controller in the presence of actual communication delays will then need to be assessed through linear and nonlinear simulations.

Coordination

For improved damping performance in the presence of communications time delays, it may be necessary to coordinate the actions of the local PSSs and designed WADC. In this work, no coordinated design or operation algorithms were implemented. Reference [83] describes a coordinated design procedure while [84] describes a coordination methodology for tuning the local AVRs and wide area damping controllers.

Appendix A

Relevant tables

A.1 Operating point of steady-state model

Comparison of load flow results between developed model and reference case scenario

Node number	Node name	Nominal voltage (kV)	Node type	Reference data		Static model		Dynamic model	
				Voltage (p.u.)	Angle (Deg)	Voltage (p.u.)	Angle (Deg)	Voltage (p.u.)	Angle (Deg)
1	Beauly	275	PV	1.000	48.75	1.000	53.79	1.000	47.85
2	Peterhead	275	PV	1.000	47.27	1.000	51.92	1.000	46.59
3	Errochty	132	PV	1.000	39.24	1.000	44.16	1.000	39.10
4	Denny	275	PV	1.000	33.26	1.000	36.25	1.000	32.90
5	Neilston	400	PV	1.000	29.55	1.000	29.85	1.000	29.17
6	Strathaven	400	PV	1.000	26.20	1.001	26.44	1.000	25.80
7	Torness	400	PV	1.000	30.68	1.000	30.82	1.000	30.36
8	Eccles	400	PQ	0.996	30.62	0.996	30.73	0.996	30.30
9	Harker	400	PQ	1.001	22.24	1.007	22.31	1.000	21.82
10	Stella West	400	PV	1.000	21.84	1.000	22.04	1.000	21.58
11	Penwortham	400	PV	1.000	15.56	1.000	15.38	1.000	15.01
12	Deeside	400	PV	1.000	14.39	1.000	13.74	1.000	13.42
13	Daines	400	PQ	0.991	12.18	0.989	12.14	0.991	11.81
14	Th. Marsh	400	PQ	0.991	15.89	0.987	16.02	0.991	15.67
15	Thornton	400	PV	1.000	17.67	1.000	17.80	1.000	17.46
16	Keadby	400	PV	1.000	16.34	1.000	16.48	1.000	16.21
17	Rattcliffe	400	PV	1.000	8.16	1.000	8.47	1.000	8.22
18	Feckenham	400	PV	1.000	7.44	1.000	7.80	1.000	7.53
19	Walpole	400	PV	1.000	7.38	1.003	7.52	1.000	7.34
20	Bramford	400	PV	1.000	3.33	1.000	3.46	1.000	3.31
21	Pelham	400	PV	1.000	4.13	1.002	4.28	1.000	4.10
22	Sundon	400	PV	1.000	3.19	1.002	3.36	1.000	3.17
23	Melksham	400	PV	1.000	2.31	1.000	2.5	1.000	2.32
24	Bramley	400	PQ	0.993	1.45	0.993	1.61	0.993	1.46
25	London	400	PV	0.995	-0.95	1.001	-0.79	0.995	-0.98
26	Kemsley	400	PV	1.000	2.26	1.000	2.37	1.000	2.25
27	Sellindge	400	Swing	1.000	0.00	1.000	0.00	1.000	0.00
28	Lovedean	400	PV	1.000	-1.03	1.001	-0.93	1.000	-1.02
29	SWP	400	PV	1.000	-1.39	1.000	-1.26	1.000	-1.39

A.2 Power system communications standards

Communications standards for power system [15], [16]

Type/Name	Description	Application area(s)
DNP3	A telecommunications standard that defines communications between client stations, RTUs and other IEDs. It is prevalent in the industry and primarily used in North America	Power system SCADA
IEC 60870-5	Standardised communication protocol defining communication profile for sending tele-control messages	Power system SCADA
IEC 62056 (superseding IEC 61107)	Set of standards for smart metering data exchange	Smart metering
IEC 61970 and IEC 61969	Providing Common Information Model (CIM): IEC 61970 works in the transmission domain and IEC 61969 works in the distribution domain	Energy management systems
IEC 61850	Flexible, open standard, communication between devices in transmission, distribution, and substation automation systems	Substation Automation
IEC 60870-6/TASE.2	Data exchange between utility control centres, utilities, power pools, regional control centres	Inter-control centre communications
IEC 62210 and IEC 62351 Parts 1-8	Define data and communication security for the communication protocols	Information Security Systems
IEC TR 62325	Framework for energy market communications	Energy Market
IEEE P2030	A guide for smart grid inter-operability of energy technology and IT operation with the electric power system (EPS)	Customer-side applications
IEEE P1901	High speed power line communications	In-home multimedia, utility and smart grid applications
ITU-T G.9955 and G.9956	Contain physical layer and data link layer specifications	Distribution Automation, Advanced Metering
OpenADR	Dynamic pricing, Demand response	Price Responsive and Load Control
BACnet	Scalable system communications at customer side	Building automation
HomePlug	Powerline technology to connect the smart appliances to HAN	Home Area Network
U-SNAP	Providing many communication protocols to connect HAN devices to smart meters	Home Area Network
ISA100.11a	Open standard for wireless systems	Industrial automation
ANSI C12.22, ANSI C12.18, and ANSI C12.19	Data structures for smart metering applications	Advanced Metering
Z-Wave	Alternative solution to ZigBee that handles the interference with 802.11/b/g	Home Area Network
M-Bus	Providing the requirements for remotely reading all kinds of utility meters	Advanced Metering
G3-PLC	Providing interoperability, cyber security, and robustness	Advance Metering
SAE J2836 and SAE J2847	Supports electric vehicle communications with grid components	Electric Vehicle

A.3 Communication service requirements for wide area applications

Wide area applications communication service requirements [13]

	Wide Area Monitoring Applications	**Latency**	**Resolution (sample/sec)**	**Comments**
Situational Awareness	Situational Awareness Dashboard	1-5 sec	1	Assess system state (Normal, Alert, Alarm)
	Real-time Compliance Monitoring	1-5 sec	1	Angle of Separation, Display Voltage, Phase, Power swing, Line loading MW/MVAR flows
	Frequency Instability Detection/Islanding	1-5 sec	25-30	
Monitoring and Decision Support	Real-time Alerts and Alarms	1-5 sec	25-30	Decision support and security assessment Help operator to respond to grid events Provide time series information Stability diagrams & Collapse margins Reposition the grid for improved security Monitoring of voltage & frequency stability Display of line temperatures
	Real-time Monitoring and Trending	1-5 sec	1	
	State Estimation	1-2 min	25-30	
	Monitoring/Assessment Voltage Stability	Few sec	25-30	
	Small-signal Stability Monitoring	Few sec	10-60	
	Line Thermal Monitoring (Overload)	Few sec	25-30	
Analysis and Static Modelling	Pattern Recognition/ Correlation Analysis	–	1	Post-incident Analysis Identify system security metrics System-level and grid asset models
	Frequency Response Analysis	–	10	
	Disturbance Analysis Compliance	–	25-30	
	Model Validation	–	25-30	
Protection and control	Adaptive Relaying	100ms	25-30	Emergency situation control and protection Closed loop system protection scheme applications
	Out-of-step Protection	100ms	25-30	
	Short-term stability control (e.g. transient stability)	100ms	25-30	
	Small-Signal stability Protection and control	100ms	25-30	
	Long-term stability control (e.g. Wide Area frequency/ voltage stability)	1-5 sec	25-30	

A.4 Relative locations of RGBN nodes in relation to core nodes

Node Number	Node Name	Closest Fibre Node	Other Close Nodes
1	Beauly	Glasgow	City Valey
2	Peterhead	Glasgow	City Valey
3	Errochty	Glasgow	City Valey
4	Denny/Bonnybridge	Glasgow	City Valey
5	Neilston	Glasgow	City Valey
6	Strathaven	City Valey	Glasgow
7	Torness	City Valey	Glasgow, Newcastle
8	Eccles	City Valey	Glasgow, Newcastle
9	Harker	Newcastle	
10	Stella West	Newcastle	
11	Penwortham	Preston	
12	Deeside	Manchester	
13	Daines	Manchester	
14	Th. Marsh/Stocksbridge	Sheffield	
15	Thornton/Drax/Eggborough	Leeds	
16	Keadby	Sheffield	Leeds
17	Ratcliffe	Derby	
18	Feckenham	Birmingham	
19	Walpole	Peterborough	
20	Bramford	Peterborough	
21	Pelham	City of London	
22	Sundon/East Claydon	Milton Keynes	
23	Melksham	Bristol	
24	Bramley	Guildford	
25	London	City of London	
26	Kemsley	City of London	
27	Sellindge	City of London	
28	Lovedean	Guildford	
29	S.W.Penisula	Bristol	

A.5 Generator information

Node	Generation Type	Rating (MVA)	P_{Gen} (MW)	Q_{Gmin} (MVAr)	Q_{Gmax} (MVAr)	Dynamic parameters (Reference no. from [54])
Beauly	Hydro	615	441.86	-254.76	244.45	H18
	Wind	569	411.82	–	–	–
Peterhead	CCGT	1932	1234.94	-491.03	1122.84	CF5-HP
	Wind	57	29.29	–	–	–
Errochty	Hydro	615	445.17	-235.11	276.13	H18
	Wind	569	324.43	–	–	–
Denny	Hydro	615	273.36	-193.15	218.27	H18
	Coal	2505	1836.33	-678.99	641.46	F19
	CCGT	278.3	208.24	-80	80	CF3-HP
	Wind	39	20.26	–	–	–
Neilston	Nuclear	1280	882.15	-439.71	431.86	N6
Strathaven	Hydro	615	66.25	-527.79	476.55	H18
	Wind	1556	805.22	–	–	–
Torness	Nuclear	1500	977.66	-469.07	681.34	N3
	Coal	1344	887.62	-336.26	346.1	F15
	Wind	350	182.35	–	–	–
Stella	CCGT	2415	1507.5	-829.63	697.17	CF5-HP
	Nuclear	1500	971.23	-539.68	559.19	N3
	Coal	590	337.68	-138.04	167.95	F18
Penwortham	Nuclear	2680	1934.42	-1063.92	1158.5	N8
	Coal	2505	1576.64	-571.46	873.22	F19
	CCGT	1449	959.98	-614.28	764.54	CF5-HP
	Wind	200	104.78	–	–	–
Deeside	Nuclear	1280	787.92	-418.12	579.98	N6
	CCGT	2415	1684.38	-948.03	1076.47	CF5-HP
	Hydro	1230	881.18	-575.52	344.48	H18
Thornton	Coal	8960	6271.80	-2527.87	3535.03	F20

Node	Generation Type	Rating (MVA)	P_{Gen} (MW)	Q_{Gmin} (MVAr)	Q_{Gmax} (MVAr)	Dynamic parameters (Reference no. from [54])
Keadby	Coal	4480	3193.49	-1289.62	1587.06	F20
	CCGT	9660	6640.24	-3917.43	4420.56	CF5-HP
Ratcliff	Coal	2360	1608	-405.94	814.23	F18
Feckenham	Coal	2360	1575.84	-534.17	884.97	F18
	CCGT	278.3	183.31	-73.58	40.02	CF3-HP
Walpole	CCGT1	3381	2287.38	-1468.98	1336.63	CF5-HP
	CCGT2	483	327.07	-162.70	162.70	CF5-HP
Bramford	Nuclear	1840.7	964.8	-523.38	621.14	N4
	CCGT	483	289.44	236.64	236.64	CF5-HP
Pelham	CCGT	966	535	-306.07	326.25	CF5-HP
Sundon	CCGT	483	323	-232.68	189.72	CF5-HP
Melksham	Coal1	4480	3032.69	-1388.27	1589.67	F20
	Coal2	448	291.85	-232.68	189.72	F15
	Nuclear	920.35	377.88	-211.43	317.76	N4
	CCGT	3381	2477.13	-1262.24	1200.81	CF5-HP
London	CCGT	2415	1708	-947.42	949.38	CF5-HP
Kemsley	Coal1	2360	1559.76	-431.35	881.44	F18
	Coal2	1344	887.62	-294.62	384.11	F15
	CCGT	2898	1981.86	-1114.64	1254.53	CF5-HP
Sellindge	Nuclear	2680	Swing	-541.79	737.03	N8
Lovedean	CCGT	1932	1229	-650.91	718.61	CF5-HP
SWP	Nuclear	1840.7	1013.84	-480.43	455.32	N4
	CCGT	1113.2	727.62	-412.03	403.35	CF3-HP

Appendix B

MATLAB codes

B.1 Participation factors, damping ratios, and frequency computation

```
function [y,V]= damp_info(x)
%Damping information.
%   This function receives the linearized system model as
%   input and returns the eigenvalues, together with information
%   about frequency in Hz and damping ratio of each eigenvalue.
%   Additionally, it returns the participation factors and the
%   matrix of right eigenvectors.


%=================================================================
temp_store=[]; % create array for temporary storage
A=x.a; % get system matrix from the lti system

% obtain right and left eigenvectors
[V,D]=eig(A);
W=inv(V);

% compute the magnitude of participation factors and normalise it to
% 100%. For complex participation factors, the magnitude is an
% of participation
Pf=abs(V.*conj(W'));
norm=sum(Pf);
norm_matrix=repmat(norm,size(A,1),1);
Pf=100*Pf./norm_matrix;

% store eigenvalues
eig_values=sum(D);

% for each eigenvalue, compute and store the frequency in Hz and the
% damping ratio in percentage
for i=eig_values
    frequency = abs(imag(i))/(2*pi);
    damping = -real(i)/abs(i) * 100;
    temp=[real(i),imag(i),frequency, damping];
    temp_store=[temp_store; temp];
end

y =[temp_store Pf'];

end
```

B.2 Eigenvalues plot

```
function eigen_plot(x)
%Plot eigenvalues on the s-plane and overlay damping ratio lines.
%   This function receives the linearized system model as
%   input and plots the eigenvalues on the s-plane.


%=============================================================
eig_values=eig(x.a); % get eigenvalues from system matrix
real_values=real(eig_values); % get real values of eigenvalues
imag_values=imag(eig_values); % get imaginary values of eigenvalues

% create a scatter plot of the real and imaginary component of eigenvalues
scatter(real_values,imag_values,'filled')
title('Original system modes')
xlabel('Real axis (Neper/s)')
ylabel('Imaginary axis (rad/s)')
hold on
sgrid([0.05,0.1],0) % overlay 5 and 10 percent damping ratio lines on plot
grid on
end
```

B.3 Wide area damping controller

```
%Controller design.
%   This script computes a strictly proper wide area damping controller
%   using h infinity synthesis method with additional pole placement
%   constraints.

%=============================================================
s = zpk('s');

% define the weighting filters as zero-pole-gain MATLAB lti sys
W1 = 10/(s + 10);
W2 = s/(s+100);

% compute a reduce order model from the original full order linear system
% using balanced model reduction
[g1,redinfo1] = schurmr('MaxError',0.005);

% compute state-space model of plant augmented with the weighting filters
P = augw(g1,W1,W2,[]);

Nmeas = 2; % number of measurement signals
Ncon = 2;  % number of control signals
Nz2 = 0;   % no signal is subject to the constraint on the h2 norm
Wz = [1 0];% set weight for only h infinity synthesis

% define the region for pole placement. The closed poles are placed within
% a conic sector lying on the left-hand of the s-plane having its apex at
% the origin and with an inner angle of 2*acos(0.1) rads, ensuring a
% minimum damping ratio of 10 percent
region = lmireg;

% compute a strictly proper wide area controller
[K,CL,normz,info] = h2hinfsyn(P,Nmeas,Ncon,Nz2,Wz,'REGION',region,'DKMAX',0);
```

B.4 Participation factor and mode shape plots

```
%Create bar plot for participation factor and compass plot for mode shape.
%   For a specified mode, this script computes the participation of the
%   generator speed deviation states in the mode. It also creates a compass
%   plot of the mode shape using the normalised speed deviation states
%   of the right eigenvector.


%================================================================
mode=519; % specify mode
index_speed=[]; % empty array for speed index
index_speed_limit=[]; % empty array for speed index with participation >= 0.1%

% store name of the states in the model in a cell array
c = linsys(1,1).StateName';

% store the right eigenvector and other pertinent information by calling
% requisite damping information function, which is described in an earlier
% script
[small_info,V] = damp_info(linsys);
number = small_info(:,5:end); % store the participation factors

% sort eigenvalues in descending order of the real part
z = complex(small_info(:,1),small_info(:,2));
[S,NDX] = esort(z);

% define a regular expression to extract the generators' speed deviation
% states from the cell array storing the name of the states
expression = '\w*Mechanical\smodel/Integrator$';
idx_speed=regexp(c,expression);

% get the index positions for the speed deviation states
iter=length(idx_speed);
for i=1:iter
    if ~isempty(idx_speed{i})
        index_speed=[index_speed i];
    end
end

% get the index positions for the speed deviation states of generators with
% participation factor greater than or equal 0.1%
check=number(mode,index_speed);
for i=1:length(index_speed)
    if  check(i)>= 0.1
        index_speed_limit=[index_speed_limit index_speed(i)];
    end
end

% get the participation of the speed deviation states (with participation
% factor >= 0.1%)sorted in descending order
[speed_S,speed_NDX]=sort(number(mode,index_speed_limit));

% get right eigenvector of speed deviation states corresponding to the
% specified mode
right=V(index_speed_limit(speed_NDX),mode);

% normalise right eigenvector with the speed deviation state having the
```

```
%Create bar plot for participation factor and compass plot for mode shape.
%   For a specified mode, this script computes the participation of the
%   generator speed deviation states in the mode. It also creates a compass
%   plot of the mode shape using the normalised speed deviation states
%   of the right eigenvector.


%================================================================
mode=519; % specify mode
index_speed=[]; % empty array for speed index
index_speed_limit=[]; % empty array for speed index with participation >= 0.1%

% store name of the states in the model in a cell array
c = linsys(1,1).StateName';

% store the right eigenvector and other pertinent information by calling
% requisite damping information function, which is described in an earlier
% script
[small_info,V] = damp_info(linsys);
number = small_info(:,5:end); % store the participation factors

% sort eigenvalues in descending order of the real part
z = complex(small_info(:,1),small_info(:,2));
[S,NDX] = esort(z);

% define a regular expression to extract the generators' speed deviation
% states from the cell array storing the name of the states
expression = '\w*Mechanical\smodel/Integrator$';
idx_speed=regexp(c,expression);

% get the index positions for the speed deviation states
iter=length(idx_speed);
for i=1:iter
    if ~isempty(idx_speed{i})
        index_speed=[index_speed i];
    end
end

% get the index positions for the speed deviation states of generators with
% participation factor greater than or equal 0.1%
check=number(mode,index_speed);
for i=1:length(index_speed)
    if  check(i)>= 0.1
        index_speed_limit=[index_speed_limit index_speed(i)];
    end
end

% get the participation of the speed deviation states (with participation
% factor >= 0.1%)sorted in descending order
[speed_S,speed_NDX]=sort(number(mode,index_speed_limit));

% get right eigenvector of speed deviation states corresponding to the
% specified mode
right=V(index_speed_limit(speed_NDX),mode);

% normalise right eigenvector with the speed deviation state having the
```

B.5 Time delay sensitivity eigenvalues locus plot

```
%Time delay sensitivity analyis.
%   This scripts stores the system matrices for different values of the
%   time constant. The one-way time delay is varied from 1 ms to 250 ms in
%   100 uniform steps. The script also plots the resultant locus of
%   eigenvalues.


%=================================================================
% full nonlinear power system model with wide area controllers
model = 'Dynamic_RGBN_PSSTransformer1';

% Specify the analysis I/Os
% Get the analysis I/Os from the model
io = getlinio(model);

% constant one-way time delays to be used in the analysis
delay = linspace(1e-3,250e-3,100);

iteration=length(delay);
store=cell(1,iteration);
load_system(model);

% for each value of time delay, linearize the model and store the system
% matrix
for i=1:iteration
    Ts=delay(i);
    sys = linearize(model,io); % Linearize the model at initial operating condition
    store{i}=sys.a; % store system matrices
end

% define colours for red-through-green colour spectrum
r=1.0;b=0.0;g=1.0;
red=linspace(0,1,round(iteration/2));
green=linspace(1,0,iteration-round(iteration/2));

% plot eigenvalues locus for increasing time delays
figure;
hold on
for i=1:iteration
    eig_values=eig(store{i});
    real_values=real(eig_values);
    imag_values=imag(eig_values);
    if i <= round(iteration/2)
        scatter(real_values,imag_values,[],[red(i),g,b],'filled')
    else
        scatter(real_values,imag_values,[],[r,green(i-round(iteration/2)),b],'filled')
    end
end
xlabel('Real axis (Neper/s)')
ylabel('Imaginary axis (rad/s)')
sgrid([0.05,0.1],0)
grid on
```

References

[1] C. B. Vellaithurai, S. S. Biswas, R. Liu, and A. Srivastava, 'Real time modeling and simulation of cyber-power system', in *Cyber Physical Systems Approach to Smart Electric Power Grid*, Springer, 2015, pp. 43–74.

[2] W. Wang, Y. Xu, and M. Khanna, 'A survey on the communication architectures in smart grid', *Comput. Networks*, vol. 55, no. 15, pp. 3604–3629, 2011.

[3] S. Jain, V. K. N., A. Paventhan, V. K. Chinnaiyan, V. Arnachalam, and P. M., 'Survey on smart grid technologies- smart metering, IoT and EMS', *Electrical, Electronics and Computer Science (SCEECS), 2014 IEEE Students' Conference on*. pp. 1–6, 2014.

[4] N. Saputro, K. Akkaya, and S. Uludag, 'A survey of routing protocols for smart grid communications', *Comput. Networks*, vol. 56, no. 11, pp. 2742–2771, 2012.

[5] A. Chakrabortty and P. P. Khargonekar, 'Introduction to wide-area control of power systems', *Am. Control Conf. (ACC), 2013*, pp. 6758–6770, 2013.

[6] Y. Chakhchoukh and H. Ishii, 'Enhancing Robustness to Cyber-Attacks in Power Systems Through Multiple Least Trimmed Squares State Estimations', *IEEE Trans. Power Syst.*, vol. 31, no. 6, pp. 4395–4405, Nov. 2016.

[7] K. Rahimi, A. Parchure, V. Centeno, and R. Broadwater, 'Effect of communication Time-Delay attacks on the performance of Automatic Generation Control', in *2015 North American Power Symposium (NAPS)*, 2015, pp. 1–6.

[8] N. Chockalingam, A. Chakrabortty, and A. Hussain, 'Mitigating Denial-of-Service attacks in wide-area LQR control', in *2016 IEEE Power and Energy Society General Meeting (PESGM)*, 2016, pp. 1–5.

[9] Y. Chakhchoukh and H. Ishii, 'Coordinated Cyber-Attacks on the Measurement Function in Hybrid State Estimation', *IEEE Trans. Power Syst.*, vol. 30, no. 5, pp. 2487–2497, Sep. 2015.

[10] M. Belivanis and K. Bell, 'Representative GB network model: Notes', *Univ. Strat. Glas. Scotl.*, 2011.

[11] K. R. W. Bell, 'Test system requirements for modelling future power systems', in *Power and Energy Society General Meeting, 2010 IEEE*, 2010, pp. 1–8.

[12] N. I. Osman, T. El-Gorashi, L. Krug, and J. M. H. Elmirghani, 'Energy-Efficient Future High-Definition TV', *Journal of Lightwave Technology*, vol. 32, no. 13. pp. 2364–2381,

2014.

[13] C. Samitier, *Utility Communication Networks and Services: Specification, Deployment and Operation*. Springer, 2016.

[14] H. W. Beaty and D. Fink, *Standard Handbook for Electrical Engineers Sixteenth Edition*. McGraw-Hill Education, 2012.

[15] V. C. Gungor *et al.*, 'Smart Grid Technologies: Communication Technologies and Standards', *IEEE Transactions on Industrial Informatics*, vol. 7, no. 4. pp. 529–539, 2011.

[16] S. Mohagheghi, J. Stoupis, and Z. Wang, 'Communication protocols and networks for power systems-current status and future trends', in *Power Systems Conference and Exposition, 2009. PSCE'09. IEEE/PES*, 2009, pp. 1–9.

[17] M. Kuzlu, M. Pipattanasomporn, and S. Rahman, 'Communication network requirements for major smart grid applications in HAN, NAN and WAN', *Comput. Networks*, vol. 67, pp. 74–88, 2014.

[18] D. Kaleshi and T. Song, 'Challenges in Smart Grid Communications', 2014.

[19] T. Yi, L. Feng, W. Qi, C. Bin, and N. Ming, 'Overview of the co-simulation methods for power and communication system', *2016 IEEE International Conference on Real-time Computing and Robotics (RCAR)*. pp. 94–98, 2016.

[20] K. Mets, J. A. Ojea, and C. Develder, 'Combining Power and Communication Network Simulation for Cost-Effective Smart Grid Analysis', *IEEE Communications Surveys & Tutorials*, vol. 16, no. 3. pp. 1771–1796, 2014.

[21] K. Mets, T. Verschueren, C. Develder, T. L. Vandoorn, and L. Vandevelde, 'Integrated simulation of power and communication networks for smart grid applications', *2011 IEEE 16th International Workshop on Computer Aided Modeling and Design of Communication Links and Networks (CAMAD)*. pp. 61–65, 2011.

[22] J. Bergmann, C. Glomb, J. Gotz, J. Heuer, R. Kuntschke, and M. Winter, 'Scalability of Smart Grid Protocols: Protocols and Their Simulative Evaluation for Massively Distributed DERs', *2010 First IEEE International Conference on Smart Grid Communications*. pp. 131–136, 2010.

[23] D. Bian, M. Kuzlu, M. Pipattanasomporn, S. Rahman, and Y. Wu, 'Real-time co-simulation platform using OPAL-RT and OPNET for analyzing smart grid performance', *2015 IEEE Power & Energy Society General Meeting*. pp. 1–5, 2015.

[24] M. Armendariz, M. Chenine, L. Nordström, and A. Al-Hammouri, 'A co-simulation

platform for medium/low voltage monitoring and control applications', *ISGT 2014*. pp. 1–5, 2014.

[25] D. Kim, Y. Yi, and S. Ha, 'Trace-driven HW/SW cosimulation using virtual synchronization technique', *Proceedings. 42nd Design Automation Conference, 2005.* pp. 345–348, 2005.

[26] K. Hopkinson, X. Wang, R. Giovanini, J. Thorp, K. Birman, and D. Coury, 'EPOCHS: a platform for agent-based electric power and communication simulation built from commercial off-the-shelf components', *IEEE Transactions on Power Systems*, vol. 21, no. 2. pp. 548–558, 2006.

[27] T. Godfrey, S. Mullen, D. W. Griffith, N. Golmie, R. C. Dugan, and C. Rodine, 'Modeling Smart Grid Applications with Co-Simulation', *2010 First IEEE International Conference on Smart Grid Communications*. pp. 291–296, 2010.

[28] R. Bottura, A. Borghetti, F. Napolitano, and C. A. Nucci, 'ICT-power co-simulation platform for the analysis of communication-based volt/var optimization in distribution feeders', *ISGT 2014*. pp. 1–5, 2014.

[29] H. Georg, S. C. Müller, N. Dorsch, C. Rehtanz, and C. Wietfeld, 'INSPIRE: Integrated co-simulation of power and ICT systems for real-time evaluation', *2013 IEEE International Conference on Smart Grid Communications (SmartGridComm)*. pp. 576–581, 2013.

[30] F. Milano and M. Anghel, 'Impact of Time Delays on Power System Stability'.

[31] M. Eremia and M. Shahidehpour, *Handbook of electrical power system dynamics : modeling, stability, and control*. John Wiley & Sons Inc, 2013.

[32] S. Ayasun and C. O. Nwankpa, 'Probability of Small-Signal Stability of Power Systems in the Presence of Communication Delays'.

[33] T. Li, M. Wu, and Y. He, 'Lyapunov-Krasovskii functional based power system stability analysis in environment of WAMS', *J. Cent. South Univ. Technol.*, vol. 17, no. 4, pp. 801–806, Aug. 2010.

[34] S. Qiang *et al.*, 'An improved power system stability criterion with multiple time delays', in *2009 IEEE Power & Energy Society General Meeting*, 2009, pp. 1–7.

[35] J. Sun and J. Chen, 'A survey on Lyapunov-based methods for stability of linear time-delay systems', *Front. Comput. Sci.*, vol. 11, no. 4, pp. 555–567, Aug. 2017.

[36] L. Shen, 'Model integration and control interaction analysis of AC/VSC HVDC system', 2015.

[37] National Grid, '2010 Seven Year Statement', 2010.

[38] G. M. Masters, *Renewable and efficient electric power systems*. John Wiley & Sons, 2013.

[39] L. L. Grigsby, *The electric power engineering handbook. Power system stability and control*. CRC Press, 2012.

[40] P. C. Krause, O. Wasynczuk, S. D. Sudhoff, and S. Pekarek, *Analysis of electric machinery and drive systems*, vol. 75. John Wiley & Sons, 2013.

[41] MathWorks Inc, 'Model the dynamics of three-phase round-rotor or salient-pole synchronous machine - Simulink - MathWorks United Kingdom'. [Online]. Available: https://uk.mathworks.com/help/physmod/sps/powersys/ref/synchronousmachine.html. [Accessed: 21-Apr-2017].

[42] M. D. Ilic and J. Zaborszky, *Dynamics and control of large electric power systems*. Wiley, 2000.

[43] 'IEEE Recommended Practice for Excitation System Models for Power System Stability Studies', *IEEE Std 421.5-2005 (Revision of IEEE Std 421.5-1992)*. pp. 1–93, 2006.

[44] F. P. Demello *et al.*, 'Hydraulic-turbine and turbine control-models for system dynamic studies', *IEEE Trans. Power Syst.*, vol. 7, no. 1, pp. 167–179, 1992.

[45] MathWorks Inc, 'Model hydraulic turbine and proportional-integral-derivative (PID) governor system - Simulink - MathWorks United Kingdom'. [Online]. Available: https://uk.mathworks.com/help/physmod/sps/powersys/ref/hydraulicturbineandgovernor.html. [Accessed: 21-Apr-2017].

[46] I. Report, 'Dynamic models for steam and hydro turbines in power system studies', *IEEE Trans. Power Appar. Syst.*, no. 6, pp. 1904–1915, 1973.

[47] MathWorks Inc, 'Model the dynamics of speed governing system, steam turbine, and multimass shaft - Simulink - MathWorks United Kingdom'. [Online]. Available: https://uk.mathworks.com/help/physmod/sps/powersys/ref/steamturbineandgovernor.html. [Accessed: 21-Apr-2017].

[48] MathWorks Inc, 'Implement three-phase dynamic load with active power and reactive power as function of voltage or controlled from external input - Simulink - MathWorks United Kingdom'. [Online]. Available: https://uk.mathworks.com/help/physmod/sps/powersys/ref/threephasedynamicload.html. [Accessed: 21-Apr-2017].

[49] M. J. Gibbard and P. Pourbeik, *Small-signal stability, control and dynamic performance of power systems*. .

[50] B. Pal and B. Chaudhuri, *Robust control in power systems*. Springer, 2005.

[51] M. Gibbard and D. Vowles, 'Reconciliation of methods of compensation for PSSs in multimachine systems', in *IEEE Power Engineering Society General Meeting, 2004.*, vol. 2, p. 1742.

[52] F. L. Pagola, I. J. Perez-Arriaga, and G. C. Verghese, 'On sensitivities, residues and participations: applications to oscillatory stability analysis and control', *IEEE Trans. Power Syst.*, vol. 4, no. 1, pp. 278–285, 1989.

[53] MathWorks, 'Simscape Power Systems - MATLAB & Simulink'. [Online]. Available: https://uk.mathworks.com/products/simpower.html. [Accessed: 15-Aug-2017].

[54] P. M. Anderson and A. A. Fouad, *Power system control and stability*. John Wiley & Sons, 2008.

[55] E. Muljadi, V. Gevorgian, M. Singh, and S. Santoso, 'Understanding inertial and frequency response of wind power plants', in *2012 IEEE Power Electronics and Machines in Wind Applications*, 2012, pp. 1–8.

[56] E. Topuz, 'Modeling the Fiber Optic Propagation Channel', in *Modeling and Simulation Environment for Satellite and Terrestrial Communications Networks: Proceedings of the European COST Telecommunications Symposium*, A. N. Ince, Ed. Boston, MA: Springer US, 2002, pp. 255–269.

[57] L. N. Binh, *Optical fiber communication systems with Matlab and Simulink models*. CRC Press, 2014.

[58] K. Dickerson and J. Dixon, 'Key Standards for BT’s 21st Century Network', *2008 2nd Electronics System-Integration Technology Conference*. pp. 63–68, 2008.

[59] G. Shen and R. S. Tucker, 'Energy-Minimized Design for IP Over WDM Networks', *IEEE/OSA Journal of Optical Communications and Networking*, vol. 1, no. 1. pp. 176–186, 2009.

[60] Y. Zhang, 'DESIGN OF WIDE-AREA DAMPING CONTROL SYSTEMS FOR POWER SYSTEM LOW-FREQUENCY INTER-AREA OSCILLATIONS', 2007.

[61] 'Blackout 2003: Final Report on the August 14, 2003 Blackout in the United States and Canada: Causes and Recommendations | Department of Energy'. [Online]. Available: https://energy.gov/oe/downloads/blackout-2003-final-report-august-14-

2003-blackout-united-states-and-canada-causes-and. [Accessed: 10-Aug-2017].

[62] M. E. Aboul-Ela, A. A. Sallam, J. D. McCalley, and A. A. Fouad, 'Damping controller design for power system oscillations using global signals', *IEEE Trans. Power Syst.*, vol. 11, no. 2, pp. 767–773, May 1996.

[63] C. He and B. Hong, 'Wide-Area Robust H 2 / H ∞ Control with Pole Placement for Damping Inter-Area Oscillation of Power System', *Introd. to Robust Control*, pp. 2101–2108, 2010.

[64] M. R. Younis and R. Iravani, 'Wide-area damping control for inter-area oscillations: A comprehensive review', *2013 IEEE Electr. Power Energy Conf. EPEC 2013*, pp. 1–6, 2013.

[65] H. Wu, K. S. Tsakalis, and G. T. Heydt, 'Evaluation of Time Delay Effects to Wide-Area Power System Stabilizer Design', *IEEE Trans. Power Syst.*, vol. 19, no. 4, pp. 1935–1941, Nov. 2004.

[66] B. Naduvathuparambil, M. C. Valenti, and A. Feliachi, 'Communication delays in wide area measurement systems', in *Proceedings of the Thirty-Fourth Southeastern Symposium on System Theory (Cat. No.02EX540)*, pp. 118–122.

[67] M. Vajta, 'SOME REMARKS ON PADÉ-APPROXIMATIONS', no. 1.

[68] L. (Luc) Wuytack and Universitaire Instelling Antwerpen., *Padé approximation and its applications : proceedings of a conference held in Antwerp, Belgium, 1979*. Springer-Verlag, 1979.

[69] L. D. Philipp, A. Mahmood, and B. L. Philipp, 'An improved refinable rational approximation to the ideal time delay', *IEEE Trans. Circuits Syst. I Fundam. Theory Appl.*, vol. 46, no. 5, pp. 637–640, May 1999.

[70] F. Lin, *Robust Control Design: An Optimal Control Approach*. 2007.

[71] K. Glover and J. C. Doyle, 'State-space formulae for all stabilizing controllers that satisfy an H∞-norm bound and relations to relations to risk sensitivity', *Syst. Control Lett.*, vol. 11, no. 3, pp. 167–172, Sep. 1988.

[72] MathWorks, 'H∞ mixed-sensitivity synthesis method for robust control loopshaping design - MATLAB mixsyn - MathWorks United Kingdom'. [Online]. Available: https://uk.mathworks.com/help/robust/ref/mixsyn.html. [Accessed: 12-Aug-2017].

[73] S. Skogestad and I. Postlethwaite, 'Multivariable feedback control analysis and design, S. Skogestad and I. Postlethwaite, Wiley, Chichester, U.K., ISBN 0-471-94277-4, xi+559 pp., 1996.', *Int. J. Robust Nonlinear Control*, vol. 8, no. 14, pp. 1237–

1238, 1998.

[74] J. Sefton and K. Glover, ‘Pole/zero cancellations in the general ∞ problem with reference to a two block design’, *Syst. Control Lett.*, vol. 14, no. 4, pp. 295–306, Apr. 1990.

[75] MathWorks, ‘Model Reduction Techniques - MATLAB & Simulink - MathWorks United Kingdom’. [Online]. Available: https://uk.mathworks.com/help/robust/gs/model-reduction-techniques.html. [Accessed: 14-Aug-2017].

[76] MathWorks, ‘State-space or transfer function plant augmentation for use in weighted mixed-sensitivity H∞ and H2 loopshaping design - MATLAB augw - MathWorks United Kingdom’. [Online]. Available: https://uk.mathworks.com/help/robust/ref/augw.html. [Accessed: 14-Aug-2017].

[77] MathWorks, ‘Mixed H2/H∞ synthesis with regional pole placement constraints - MATLAB h2hinfsyn - MathWorks United Kingdom’. [Online]. Available: https://uk.mathworks.com/help/robust/ref/h2hinfsyn.html. [Accessed: 14-Aug-2017].

[78] E. Vaahedi, *Practical power system operation*. .

[79] S. F. Bush, *Smart grid - communication-enabled intelligence for the electric power grid*. .

[80] S. Mohagheghi, G. K. Venayagamoorthy, and R. G. Harley, ‘Optimal Wide Area Controller and State Predictor for a Power System’, *IEEE Trans. Power Syst.*, vol. 22, no. 2, pp. 693–705, May 2007.

[81] H. Liu *et al.*, ‘ARMAX-Based Transfer Function Model Identification Using Wide-Area Measurement for Adaptive and Coordinated Damping Control’, *IEEE Trans. Smart Grid*, vol. 8, no. 3, pp. 1105–1115, May 2017.

[82] A. Thakallapelli, S. J. Hossain, and S. Kamalasadan, ‘Coherency based online wide area control of wind integrated power grid’, in *2016 IEEE International Conference on Power Electronics, Drives and Energy Systems (PEDES)*, 2016, pp. 1–6.

[83] D. Molina, G. K. Venayagamoorthy, and R. G. Harley, ‘Coordinated design of local and wide-area damping controllers for power systems using particle swarm optimization’, in *2013 IEEE Power & Energy Society General Meeting*, 2013, pp. 1–5.

[84] H. Bevrani, M. (Electrical engineer) Watanabe, and Y. Mitani, *Power system monitoring and control*. .

[85] W. H. A. Schilders, H. A. van der Vorst, and J. Rommes, *Model order reduction : theory, research aspects and applications*. Springer, 2008.

[86] G. Obinata and B. D. O. Anderson, *Model Reduction for Control System Design*. Springer London, 2001.